University of Milano - Bicocca

PhD School in Nanostructure and Nanotechnologies

XXVIII Cycle

Enhanced Brain Targeting of ApoE – functionalized Lipid Nanoparticles

Supervisor: **Dr. Giulio Alfredo Sancini**

PhD coordinator: **Prof. Gianfranco Pacchioni**

PhD dissertation of:

Roberta Dal Magro

Academic Year 2014/2015

To my grandmother

Contents

Abstract

The blood-brain barrier (BBB) plays an important role in maintaining the homeostasis of the central nervous system and in protecting the brain from potentially harmful endogenous and exogenous compounds. Nevertheless, it represents also the major obstacle for the diagnosis and the therapy of brain diseases. One of the most promising strategies to overcome the limited BBB penetration of drugs and contrast agents is based on nanoparticles (NPs). Lipid based NPs, mainly liposomes (LIP) and solid lipid nanoparticles (SLN), have several advantages in terms of biocompatibility, non-immunogenicity, non-toxicity; they can be used as carrier systems and they have a prolonged circulation time in the bloodstream. Moreover, their surface can be easily modified with ligands in order to obtain a site-specific targeting. The aim of the present investigation is related to the evaluation of the ability of NPs functionalized with Apolipoprotein-E (ApoE) or a peptide derived from ApoE (mApoE) to cross the BBB and to reach the brain parenchyma. The thesis is structured in three main experimental sections. In the first one (chapter II), the interaction of SLN covalently coupled with mApoE (SLN-mApoE) and brain capillary endothelial cells (hCMEC/D3) has been evaluated. SLN without surface-located peptide displayed less membrane accumulation and cellular uptake compared to SLN-mApoE. Moreover the presence of mApoE significantly enhanced SLN permeability across the BBB *in vitro* model ([^{14}C]-DPPA permeability=5.7±0.3×10^{5} cm/min, [^{3}H]-CE permeability=6.9±0.4×10^{-5} cm/min). The *in vivo* biodistribution of SLN has been evaluated by means of fluorescent microscopy tomography system, and the here obtained results demonstrated that the intratracheal (IT) administration of SLN-mApoE significantly increased SLN-related fluorescence in the brain compared to IV and IP administrations. In chapter III, the intratracheal instillation has been investigated as an alternative, non-invasive delivery route for LIP to reach the brain. It has already been proven that LIP functionalized with phosphatidic acid (PA) and mApoE (mApoE-PA-LIP) and administered by intraperitoneal (IP) or intravenous (IV) injection, are able to cross the BBB *in vivo*. The results here obtained showed that mApoE-PA-LIP were able to cross the pulmonary epithelium *in vitro* and to reach the brain (0.6 μg PA/g brain) *in vivo.* Moreover, IT instillation of mApoE-PA-LIP to Alzheimer's disease mice significantly decrease total brain Aβ (-60% of Aβ; p<0.05) respect to untreated mice. Finally, chapter IV focuses on an alternative strategy to functionalize the surface of solid lipid nanoparticles, here

referred as Lipid NPs, with ApoE by mimicking an artificial apolipoprotein-E mediated protein corona. Polysorbate 80-coated Lipid NPs, produced by hot high pressure homogenization technique, were decorated with ApoE3 or ApoE4 exploiting ApoE adsorption to polysorbate 80, and their accumulation in the brain was assessed. Thirty minutes after systemic administration, Lipid NPs-ApoE4 reached the brain, distributing in the brain microvessels as well as in the brain parenchyma.

These results suggest that the functionalization of both LIP and SLN with mApoE peptide increases NPs brain targeting and that IT instillation could be exploited as an alternative route for the administration of NPs specifically designed for brain targeting. Moreover, the ApoE-mediated artificial protein corona effect could be an elegant strategy to increase SLN-BBB crossing.

Chapter I

Introduction

Neurological disorders represent one of the main causes of mortality, thus producing an important high social impact. Among this class of diseases that affect central nervous system (CNS), Alzheimer and other dementias are responsible for the 2.84% of deaths globally. [1] Due to the incomplete brain biological knowledge, together with the peculiar anatomical and physiological features that characterize the brain and the central nervous system in general, the pharmacological treatment of brain disease is still a difficult task.

The main obstacle is represented by the blood-brain barrier (BBB), which regulates brain influx and efflux from the bloodstream of endogenous and exogenous compounds. Because of the peculiar properties of endothelial cells lining brain capillaries, most of potential CNS drugs do not cross the BBB or do not reach the brain parenchyma in therapeutic concentration. [2]

The consequence of the limited passage of drugs from the blood to the brain is that the majority of neurological disorders are currently untreatable. [1] This problem underlie the urgent need to develop not only new effective therapeutics but also new modalities of drug delivery to overcome the limited CNS penetration of drugs. [2]

1.1 THE CENTRAL NERVOUS SYSTEM BARRIERS

The central nervous system is a delicate environment whose homeostasis is finely regulated by a set of barriers. The CNS barriers, collectively known as blood-brain interfaces, are composed of specialized cells that allow the correct CNS development and physiology. [3] Since proper neuronal function necessitates a highly regulated extracellular environment and a wide range of chemical we consume in our diet are quite neurotoxic, it is of mainly importance that the blood-brain interfaces act as dynamic regulators of ion balance and nutrients transport and as barriers to potentially harmful endogenous and exogenous compounds. [4]

The blood-brain barrier separates the brain parenchyma from the systemic blood circulation. It is formed by the endothelium of cerebral microvessels and has an estimated surface area of 100 cm^2 per gram of brain tissue in adult mammal.

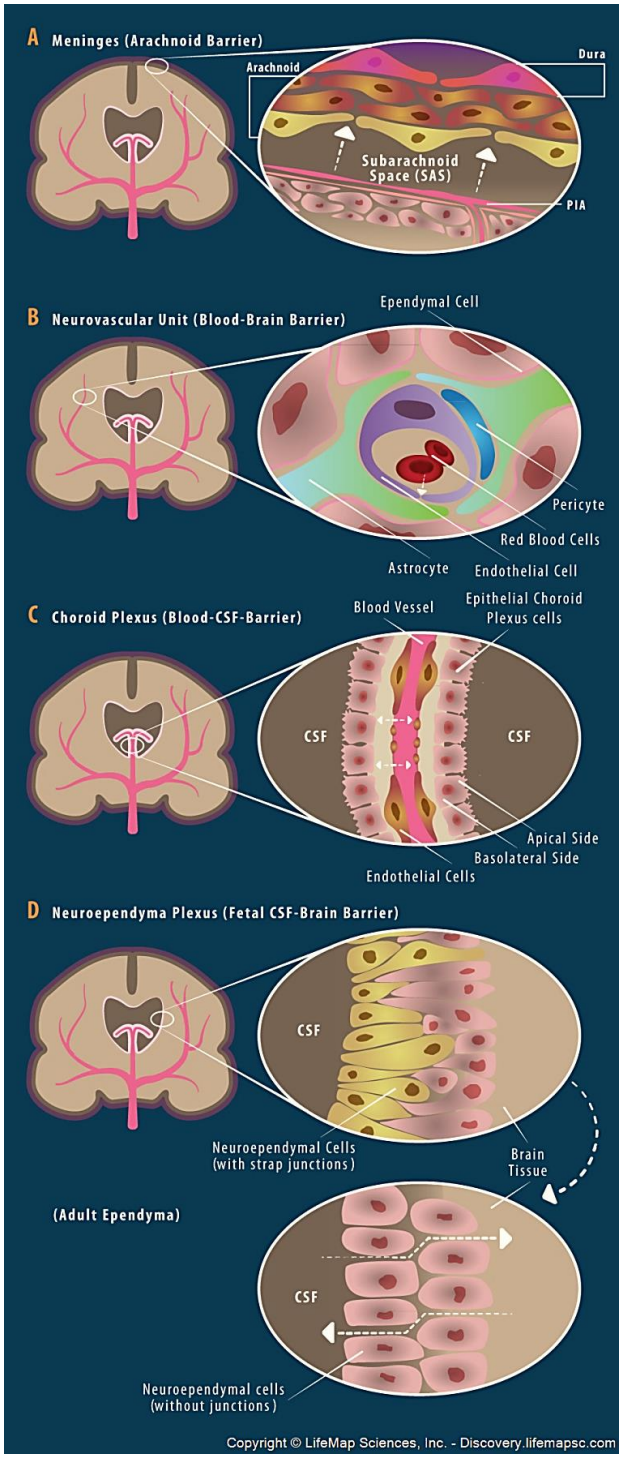

Figure 1.1. Cellular interfaces in the central nervous system.

The tight endothelium of the BBB characterizes the capillaries of both grey and withe matter structures, including those of the hypothalamus. [3] On the contrary, the capillaries of circumventricular organs (CVO) possess *fenestrae* and have a low diffusional resistance. The presence of permeable capillary in these structures allows blood-borne signals to diffuse into the brain and stimulate sensory neurons, and brain-borne signals to enter the systemic circulation and exert peripheral somatic effects. [5]

Nevertheless the surface area of CVO capillaries is modest compared to the surface developed by the BBB, thus not representing a significant route of entry for blood-borne compounds into the whole CNS. The blood-ventricular cerebrospinal fluid barrier (BCSFB), the ependyma and the arachnoid interface (Figure 1.1) represent the other CNS interfaces.

The BCSFB is composed of the tight polarized epithelium of the choroidal plexus and separates the blood from the ventricular cerebrospinal fluid (CSF). Instead, the ependyma and the arachnoid membrane represent the CSF-brain interfaces. The former separates the brain parenchyma from the CSF and is characterized by the lack of tight junctions between the ependymal cells, the latter is the interface between subarachnoid CSF and the *dura mater*. [3]

1.2 THE BLOOD-BRAIN BARRIER

The blood-brain barrier was first described by Paul Ehrlich in 1904, [6] who noted that water-soluble dyes injected in the system circulation failed to reach the brain and the spinal cord, while staining most other organs in the periphery. Few years later, Ehrlich's student Goldmann proved that trypan blue was able to stain the nervous tissue but not peripheral organs when injected in the CSF. [7] These findings suggested for the first time the presence of a barrier between the CNS and the circulatory system preventing the free diffusion of the dyes. Nevertheless, the perception of the BBB as a dynamic interface not only stimulated by vascular signal, but signals from the parenchyma as well, and its involvement in the majority of CNS disorders are more recent evidences and are currently under investigation. [8] The BBB consists of specialized brain capillary endothelial cells (BECs), pericytes, basal lamina and astrocyte end-feet. All together these cells constitute the "neurovascular unit" (NVU), a complex structure where a multiplicity of cells associates and communicates to carefully regulate exchanges between the blood and the interstitial fluid of the brain (Figure 1.2)

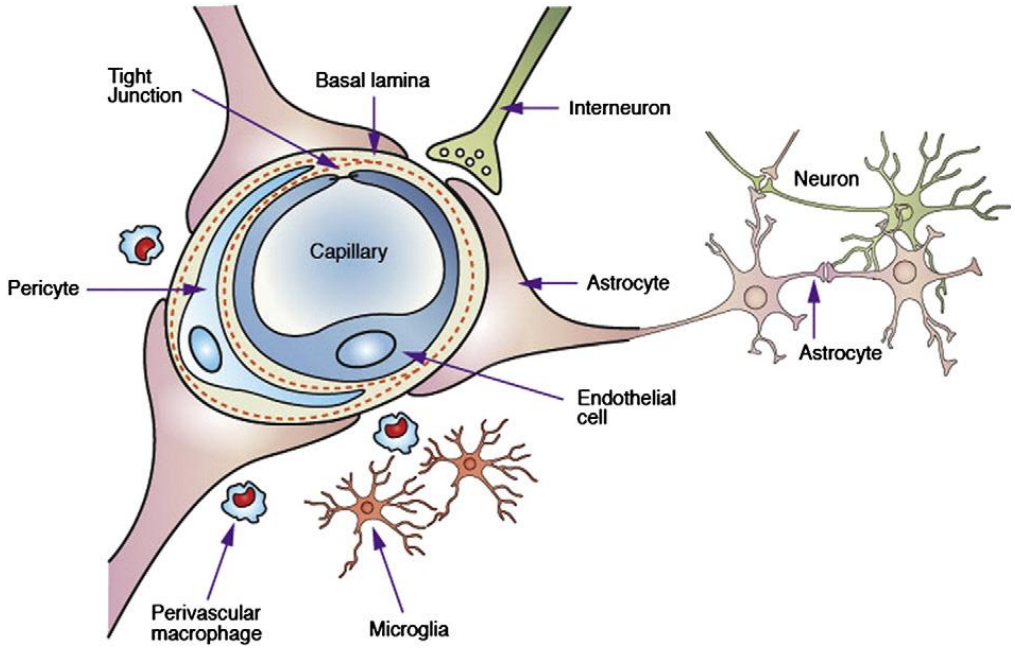

Figure 1.2. The neurovascular unit. [9]

1.2.1 BRAIN CAPILLARY ENDOTHELIAL CELLS

BECs are the first interface between the blood and the nervous tissue since they line the capillary lumen by forming a monolayer. Unlike the endothelial cells at the periphery, BECs at the BBB have increased number of mithocondria, lack fenestrations, reduced number of pinocytotic vesicles and they are characterized by the presence of tight junctions (TJ) between adjacent cells. [4]

TJ are the major responsible for the low paracellular permeability across the BBB. They are located in the apical region of lateral plasma membranes and are composed of a set of interacting proteins, which mediates a tight apposition between the membranes of adjacent cells, thus limiting the passage of selected inorganic ions, solutes and water via this route. Moreover, the presence of TJ allows the polarization of BECs and the separation of membrane proteins between the luminal and abluminal domains of the cells. [3] The transmembrane proteins of the TJ at the BBB are occludin, claudins and junctional adhesion molecule (JAM)-1 (Figure 1.3). Occludin is a 60-65 kDa protein made up of four transmembrane domains, cytoplasmic amino and carboxyl terminals and two extracellular loops, which provide the TJ gate-like structure. The C-terminal domain associates with F-actin on the cytoplasmic

side of TJ via zonula occludens (ZO)-1 and ZO-2. [10] Nevertheless, results obtained by using occludin-deficient epithelial cells and occludin-deficient mice indicated that this protein is not essential for the formation of TJ [11,12], thus suggesting a role for occludin in TJ control and regulation rather than in establishment. [13]

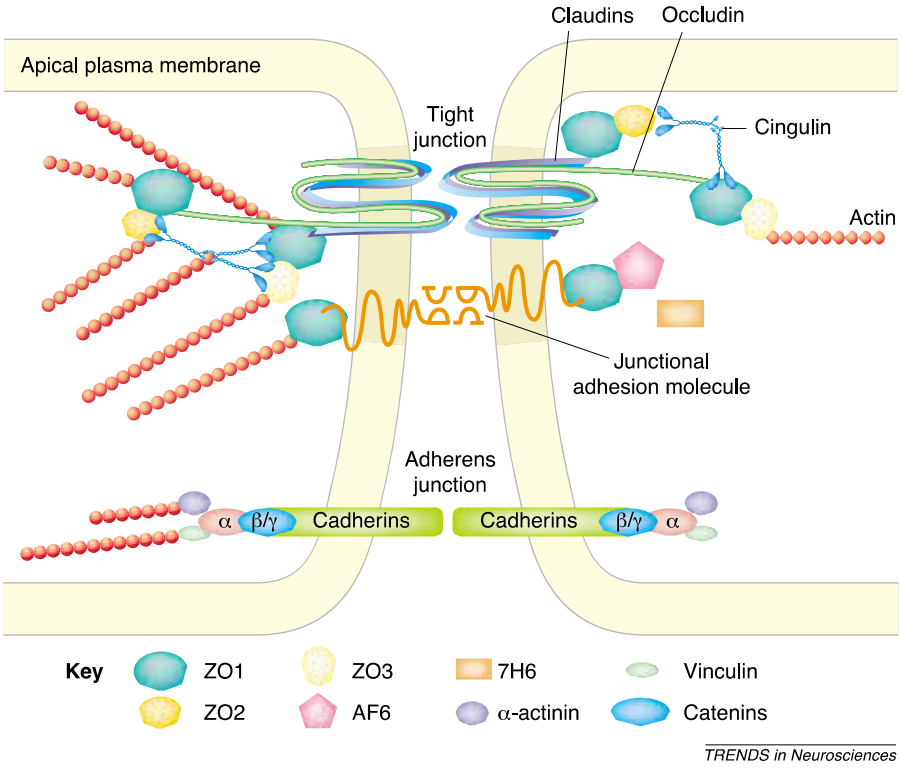

Figure 1.3. Components of tight junctions at the blood-brain barrier. [14]

Claudins are 21-28 kDa transmembrane proteins. Humans and mice possess 24 members of this family and claudin-5 has the highest expression at the BBB. Claudins possess four transmembrane domanis, amino- and carboxy-terminal cytoplasmic domains, and a short cytoplasmic turn. The PDZ-domain binding motif located at the carboxyl terminus binds to the PDZ domains of ZO-1 and ZO-2, while the extracellular loops account for homotypic and heterotypic interactions between cells. [13,15] Moreover, the extracellular domains provide paracellular charge selectivity, so that each type of claudin regulates the diffusion of specific ions. [10] In *vitro* and in *vivo* gain-of-function and loss-of-function studies demonstrated that claudins are essential for the generation of TJ strands. [13]

Finally, JAMs are the last family of transmembrane proteins composing the TJ. They are members of the Ig superfamily and are characterized by a transmembrane domain, an extracellular carboxy-terminal domain and a cytoplasmic amino-terminal tail. JAM-1 is a 40 kDa protein involved in the early attachment of adjacent cell membranes by both homophilic and heterophilic interactions. [16] On the contrary, JAM-2 and JAM-3 may have a role in leukocytes recruitment. [17]

In addition to these transmembrane proteins, TJ are also made up of several cytoplasmic accessory proteins, which mediate the interaction between transmembrane proteins and the cytoskeleton. ZO-1, ZO-2 and ZO-3 are members of the membrane-associated guanylate kinase-like (MAGUK) homolog family. They link transmembrane proteins of the TJ to the cytoskeleton and act also as signalling molecules able to translocate to the nucleus in response to stress. AF6 has two Ras-associated domains and participates in the regulation of cell–cell contacts via interaction with ZO-1. The interaction between ZO-1 and AF6 is inhibited by Ras activation, suggesting a role of Ras pathway in the modulation of TJ. [18] 7H6 antigen is a phosphoprotein whose role in TJ function is not completely known. However, it has been hypothesized that ATP depletion induces 7H6 dissociation from the TJ complex resulting in enhanced paracellular permeability. Finally, cingulin is a double-stranded myosin-like protein localized at the cytoplasmic surface of TJ. It binds preferentially to ZO proteins at the globular head and to other cingulin molecules at the globular tail and appears to act as a scaffolding protein by linking TJ accessory proteins to the cytoskeleton. [14]

The tight apposition between brain capillary endothelial cells is also mediated by adherens junction (AJ) and possibly gap junctions. Together with TJ, AJ are responsible for the low paracellular permeability across the BBB. The main component of AJ is vascular endothelial (VE)-cadherin, a calcium-regulated protein that mediates the attachment of adjacent cell membranes via homophilic interactions. Stabilization of the junctional complex is achieved by the linkage of VE-cadherin cytoplasmic tail to β-catenin, which indirectly interacts with F-actin via α-catenin, α-actinin and vinculin. [4]

1.2.2 PERICYTES

Pericytes are spread along the abluminal surface of vascular endothelium (one pericyte for every 5-6 BECs). They communicate with all the other cellular components of the NVU and are involved in the

regulation of microcirculation, neoangiogenesis and inflammation. Indeed pericytes have a direct role in maintaining BBB permeability by promoting tight junctions formation and by inhibiting endothelial transcytosis of macromolecules. [19] Moreover peryctes regulates microvascular blood flow in the CNS in response to local neuronal activity. [20] Pericytes are also involved in neovascularization. It has been shown that pericytes (i) travel to the vascular sprouts to regulate endothelial cell proliferation, (ii) attach to newly formed vessels for vascular maturation, (iii) contribute to the basement membrane formation and stabilization, and (iv) assist in forming the blood–brain barrier. Finally pericytes produce inflammatory markers in response to immune stimuli, allowing leukocytes migration across vascular wall. [21]

1.2.3 ASTROCYTES

It is well known that astrocytes regulate the transport of nutrients from the blood flow to the nervous tissue. Neuronal activity induces an increment of Ca^{2+} levels in peri-synaptic astrocyte end-feet that propagates throughout astrocytes reaching astrocytic foot processes surrounding the capillary wall. In this site, Ca^{2+} activates phospholipase A_2 that in turn trigger synthesis of specific vasoactive mediators. Prostaglandin E_2 and epoxyeicosatrienoic acids induce vasodilatation, whereas 20-hydroxyeicosatetraenoic stimulates vasoconstriction. Moreover, Ca^{2+} increase in astrocyte end-feet trigger the activation of other molecular pathways involved in vascular tone modulation. [21] In addition, the expression of aquaporine-4 on the astrocytic processes has been described, thus suggesting the involvement of this specialized membrane domains in the regulation of brain water homeostasis. [22,23]

1.2.4 THE BASEMENT MEMBRANE

The basement membrane is a complex extracellular matrix made up of collagen type IV, elastin, fibrillin, laminin and fibronectin. The composition of this acellular membrane is regulated by metalloproteinases and plasmin. [24] The basement membrane surrounds BECs and pericytes and does not only maintain capillary vessels morphology, but it also allows the correct BBB function. The disruption of basement membrane is in fact related to severe barrier compromise, as observed in different neurodegenerative diseases. [8, 25]

In addition to the basement membrane that engulfs the BECs, a second membrane, called the glia limitants, has been described at the CNS. Together with the BECs basement membrane, this astroglial basement membrane delimits a perivascular space, whose function is still unclear, between the astrocytic end feet and the vascular wall. [8]

1.3. TRANSPORT SYSTEMS OF THE BBB

Due to the presence of tight junctions, molecules can cross the BBB only by exploiting the transport mechanisms expressed on BECs membranes. The blood-to-brain influx systems allow nutrients to reach the nervous tissue, whereas the brain-to-blood efflux mechanisms clean out the brain from metabolites and neurotoxic compounds. The transport systems of the BBB can be classified in: i) ionic transport systems; ii) Na^+ dependent and independent transporters; iii) receptor-mediated trancytosis; iv) adsorptive-mediated transcytosis and v) active efflux pumps (Figure 1.4). The transport proteins are present both on the luminal and abluminal membrane of BECs, even though some transporters are preferentially expressed on one wall rather than the other. [8]

The ion channels (i) have an important role in the regulation of cerebral ionic balance, which is essential for neuronal activity. Na^+ levels are mainly controlled by Na^+-K^+-ATPase pumps and Na^+-H^+ counter-transporters at the abluminal membrane of BECs, and by Na^+-K^+-$2Cl^-$ cotransporters at the luminal wall. These transport systems regulate brain Na^+ and K^+ homeostasis, thus allowing the correct neuronal depolarization. [3,8]

Small organic compounds can only cross the BBB by means of plasma membrane transporters. Cerebral Na^+ independent transporters (ii) include members of the organic anion transporting polypeptides family (such as Oatp2, Oatp3 and Oatp14) and two organic anion transporters (OAT3 and RST). Oatp transporters are involved in the trafficking of bile salts, organic dyes, steroid conjugates, thyroid hormones and neuroactive peptides across the BBB, whereas OAT3 removes neurotransmitter metabolites and dopamine main metabolite, homovanillic acid, from the brain.

Moreover, glucose is transported toward the BBB by Glut1-mediated facilitative diffusion. The Glut1 system is located on both BECs membranes, but it is more concentrated on the luminal wall.

Other members of Na^+ independent transport systems are L1 transporters and the y+ system, which are expressed on both BECs membranes and mediate essential neutral amino acid and cationic amino acid,

respectively, crossing of the BBB. Instead X_G^- system, SNAT3 and SNAT5 are located only at luminal membrane and control acidic amino acids and glutamine transport, respectively. [8]

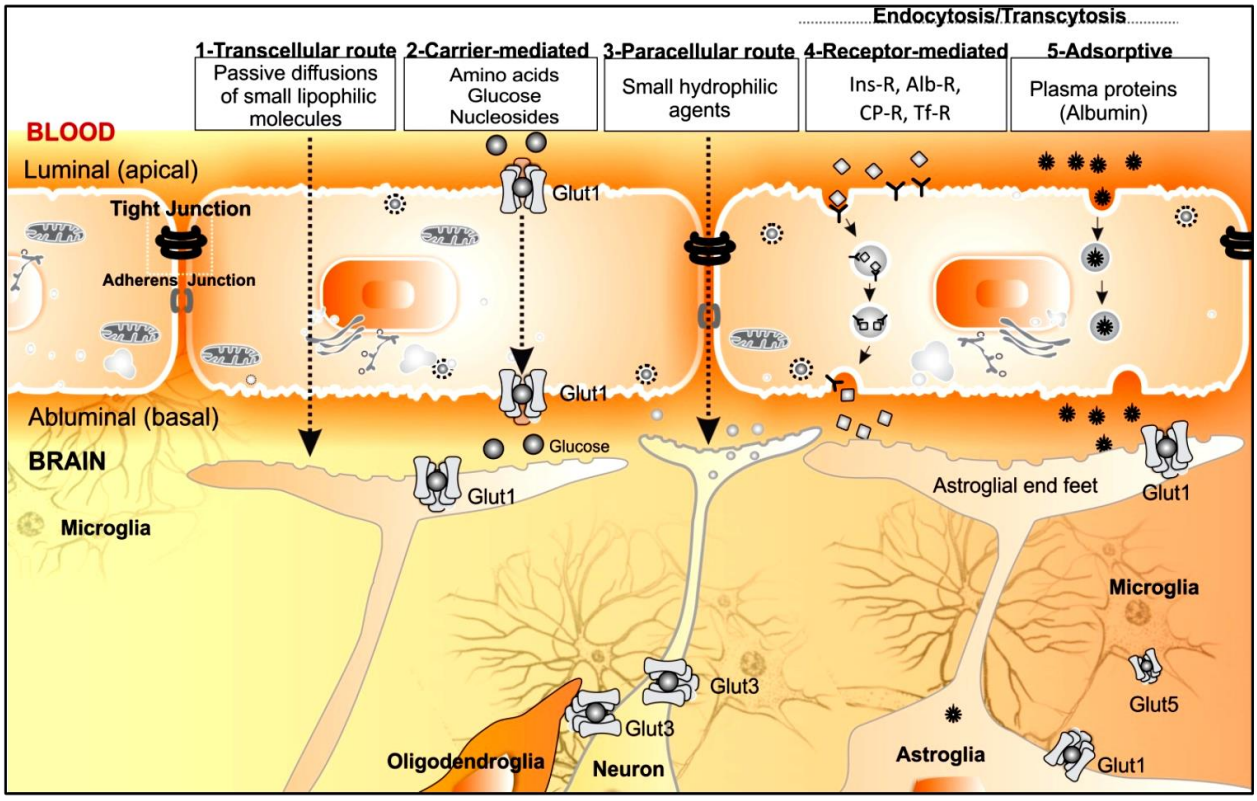

Figure 1.4. Mechnisms of transport at the BBB. [26]

In addition to Na+ independent transporters, Na+ dependent carriers (iii) are expressed at the BBB, where they play an essential role in the removal of nonessential amino acids and neurotransmitters from the brain, thus preventing their accumulation. Among these transporters, EAAT (excitatory amino acid transporters) is involved in brain-to-blood transport of glutamate avoiding potential excitotoxicity.[8]

Brain capillary endothelial cells express also a number of receptors on their surface, such as insulin receptor, transferrin receptor and LDL receptors, able to transport specific nutrients across the BBB by means of intracellular vesicles (iv). [8] On the contrary, some cationic proteins, for instance albumin, do not recognize a specific receptor on BECs membrane, but can interact with basic molecules on the

luminal/abluminal wall of brain capillaries and undergoing nonspecific adsorptive trancytosis processes. [27] Finally, efflux mechanisms are highly represented at the BBB (vi) and are the main responsible of drugs and xenobiotics efflux from the brain. The efflux pumps belong to the ATP-binding cassette superfamily and are expressed on the luminal membrane of BECs. At the BBB environment, this family is represented by the Breast Cancer Resistence protein (BCRP), the Multidrug Resistant Proteins (MDRs) and the MDR related proteins (MRPs). P-glycoprotein (P-gp) is the main MDR and it recognizes a broad spectrum of substrates, including a wide range of anticancer agents and other lipophilic drugs. [8, 26] Therefore, efflux systems represent an obstacle for drugs accumulation in the brain.

1.4. DRUG DELIVERY TO CNS

Due to the presence of a tight vascular endothelium, most pharmaceuticals are excluded from CNS entry. Indeed, only small hydrophilic drugs with a mass lower than 150 Da and highly hydrophobic compounds with a molecular weight lower than 400-600 Da can cross the BBB by paracellular and passive diffusion, respectively. [1] It is assumed that a good candidate drug should have neutral charge, a log octanol/water partition coefficient between 0.5 and 6.0 and a polar surface area lower than 80 $Å^2$. Neverthless several small highly lipophilic compound with ideal features for the diffusion across the BBB, are recognize by efflux pumps and extruded from BECs, as mentioned above. [5]

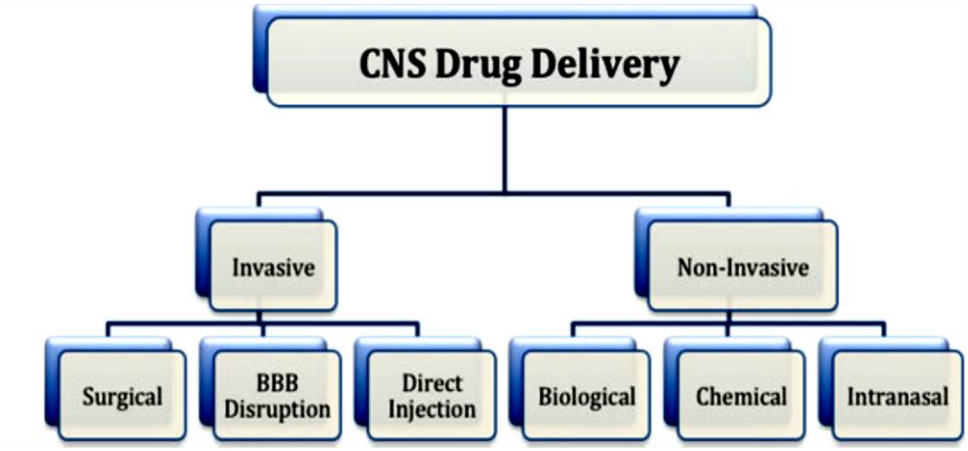

Figure 1.5. Classification of CNS drug delivery strategies. [2]

Different strategies have been developed to overcome the BBB and increase drug bioavailability at the CNS. The drug delivery techniques can be divided in two main categories: invasive and non-invasive approaches (Figure 1.5).

1.4.1 INVASIVE APPROACHES

Invasive techniques involve intracerebral injection and BBB modulation. The former consists in the insertion of a small catheter into the target region of the brain. Convection-enhanced drug delivery (CED) allows a direct injection of the drug in the CNS, thus bypassing the BBB and allowing drug accumulation at the target site. This approach establishes a pressure gradient that causes the drug penetration throughout a large volume of brain tissues, while minimizing systemic side effect since drugs are excluded from entering systemic circulation. The main limitation of this technique, in addition to its invasiveness, is the risk of infections induced by the canula. [2, 5, 28] This strategy has currently been tested in clinical for the treatment of glioblastoma. [29]

The modulation of BBB permeability is another invasive approach based on tight junctions reversible opening. Osmotic BBB disruption, by means of hypertonic mannitol solution, has been applied for several years for the treatment of brain tumors. [30,31] Mannitol is usually administered by injection into a carotid artery and it increases paracellular permeability by inducing cell shrinkage. Another strategy to modulate tight junction is the treatment with bradykinin, a peptide that binds B2 receptor and activate an intracellular pathway that leads to the disarrangement of tight junctions structure. However B2 receptors are not only located at the luminal membrane of BECs but they are expressed in several peripheral organs. Therefore, both these approaches are nonselective for the treatment of CNS diseases.[5]

To overcome the lack of selective drug delivery, ultrasound have been utilized in preclinical studies to induce a localized BBB opening. [32] In this case, the specific BBB disruption is achieved by injecting microbubble into systemic circulation and by focusing an ultrasound wave on the targeted BBB region, thus causing microbubbles oscillation and BBB opening. [5] Microbubbles are composed of a lipid or polymeric matrix, a stabilized gas core and have a dimension less than 10 μm. [33] When they are exposed to a sound wave, they oscillate around their equilibrium radius. This behaviour is known as acoustic cavitation. [34] Depending on the ultrasound wave intensity and on the microbubbles properties, acoustic cavitation can increase vascular permeability, but the exact mechanisms are still unknown. [33]

The main disadvantage of these approaches is therefore related to neurotrasmitters, antibodies and other potentially damaging compounds entry in the CNS, due to the increased BBB permeability. [2, 5]
The above mentioned techniques require hospitalization and are too invasive for long-term therapy, therefore they are unsuitable for the treatment of neurodegenerative disorders. [2]

1.4.2 NON-INVASIVE APPROACHES

Non-invasive CNS drug delivery strategies include chemical modification of therapeutic compounds, intranasal drug delivery and biological drug delivery.
Prodrug approach is based on chemical modification of the drug structure to increase its lipid solubility. A good example is represented by heroine, a prodrug for morphine that has an increased BBB penetration compared to morphine but once into the brain is converted into morphine, the active polar compound that remained locked in the CNS. [5] However, increasing the lipophilicity of a drug can also enhance both plasma proteins binding, thus causing the sequestration by reticuloendothelial system (RES) [5], and prodrug affinity for BBB efflux mechanisms. [35]
Chemical modification of drugs in order to exploit BECs endogenous transporters has also been explored. For instance, the L1 system, which manages neutral amino acid transport across the BBB, allows also L-DOPA entry in the CNS for the therapy of Parkinson's disease. L-DOPA exploits L1 transporter to reach the brain, wherein it is converted in its active form (dopamine). [2]
The drug delivery to CNS via the olfactory epithelium represents a further non-invasive strategy, even if the mechanisms involved in nose-to-brain transport have not been completely elucidated yet.
A first possibility is that therapeutic agents, which can be administered as liquids or aerosol, could penetrate through the olfactory mucosa, enter channels created by olfactory ensheathing cells surrounding the olfactory nerve and reach the CSF and the olfactory bulb. An additional hypothesis is that drugs could be uptaken by the olfactory nerves and transported by retrograde axonal cytoplasmic flow into the CNS. [5, 36] The former mechanism provides a rapid drug delivery to the brain and is supported by different studies; the latter is a slow process taking several hours for a drug to reach the olfactory bulb. The involvement of the trigeminal nerve in the intranasal delivery has also been reported. [36]
The intranasal administration of insulin is currently under investigation for the treatment of Alzheimer's disease and it represents a promising strategy to avoid peripheral effects. [36, 37]

Nevertheless, the olfactory bulb has a lower surface of adsorption compared to the BBB and limited amounts of drugs can reach the brain via this route, making these the main limitations of this technique.[1]

Another strategy to enhance drug delivery to the brain is to take advantage of receptor-mediated trancytosis by conjugating an active drug molecule to an endogenous transport substrate or to antibodies.

Examples are given by the linking of an active peptide to monoclonal antibodies (mAb) for transferrin or insulin receptors. OX26 antibody, which specifically binds transferrin receptor at a different epitope from transferrin, has been proposed as a useful strategy to deliver active peptides to the brain, [38, 39] as well as mAb to insulin receptor have been successfully tested. [40] This "Trojan horse" strategy has also been applied to conjugate drugs to cell-penetrating peptides (CPPs), short sequences of amino acids enriched in positively charged residues. A well-known CPP, Human Immunodeficiency Virus type 1 (HIV) transactivator of transcription (TAT), as well as penetratin and other CPPs interact with the negatively charged glycoproteins on BECs membrane and mediate the translocation of the conjugated drug across the BBB by means of adsorptive-mediated transcytosis. [5, 41]

The main limitation of these "Trojan horse" approaches is that they are based on the conjugation of one active molecule to one mAb, thus resulting in a quite low transport across the BBB. [5]

Along with drug conjugation to proteins or peptides, also nanoparticle-based drug delivery systems have been developed as suitable vehicles for overcoming the limited BBB penetration of conventional drugs. [42]

1.5. NANOTECHNOLOGY AND NANOMEDICINE IN DRUG DELIVERY

The term nanotechnology refers to a scientific area involved in the manipulation of atoms and molecules leading to the production of materials and devices in the nanometer scale range and that show peculiar properties. [43, 44]

Nanomedicine is the application of nanotechnology to healthcare, mainly in the field of diagnosis, drug delivery and tissue regeneration. Among different devices, nanoparticles (NPs) technology is gaining increasing interest and is emerging as a powerful strategy for the treatment of several pathologies.

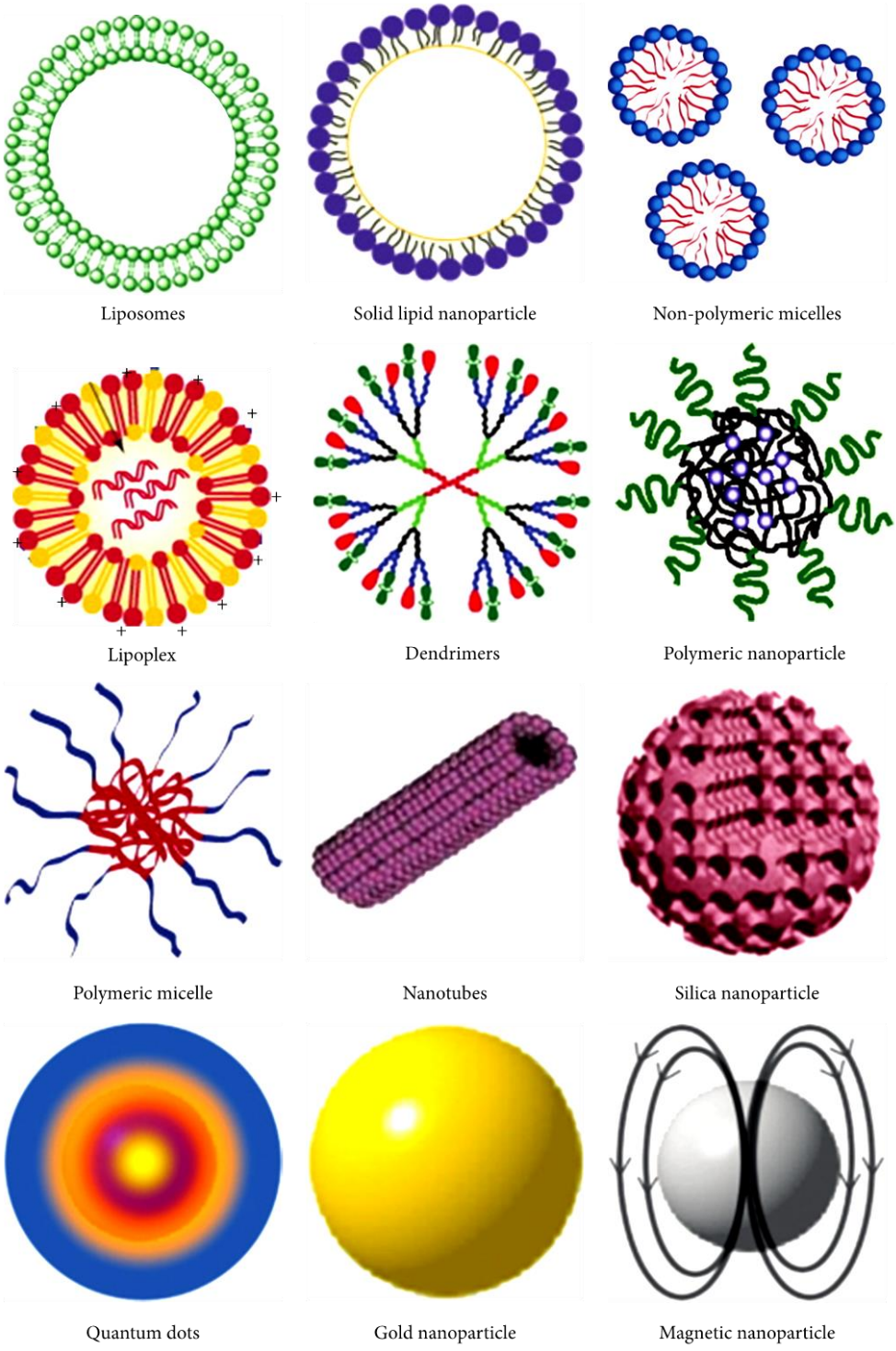

Figure 1.6. Nanoparticles for biomedical application. [1]

Nanoparticles are colloidal objects with an ideal dimension between 1 and 100 nm. They are characterized by a large surface-area-to-volume, thus allowing the surface functionalization with multiple copies of a ligand. Moreover, they can deliver hydrophobic and/or hydrophilic molecules (depending on NPs composition and structure) across biological barriers to the target site. The chemical and biological stability of NPs can be controlled and they can exploit different routes of administration, including oral, parenteral, nasal, pulmonary route and so on. [1]

Currently several kinds of nanoparticles with different phsyco-chemical properties have been tested for biomedical applications (Figure 1.6).

NP fate and ability to overcome biological barrier depend on different features, including NP shape, size, surface charge and surface functionalization. [42]

Nanoparticles size is critical for avoiding a rapid clearance. Renal filtration is responsible for the elimination of nanoparticles with a diameter below 5 nm. On the contrary, reticuloendothelial system, liver and spleen account for the clearance of particles larger than 200 nm. Therefore, 100 nm nanoparticles have a prolonged circulation time. In addition, the shape and the surface charge influence NPs fate. It has been demonstrated that neutral or negatively charged NPs have longer circulation half-lives compared to positively charged NPs. Indeed the latter have a higher affinity for serum proteins, thus allowing the formation of the protein corona and the elimination by RES. NPs shape conditions instead their margination to vessel walls, which is essential for NPs interaction with receptor express on the endothelium. [42] Blood flow dynamic simulations demonstrate that discoidal NPs are more prone to marginate to the vascular wall compared to spherical NPs. [45, 46]

Finally, NPs circulation lifetime is strongly affected by serum proteins absorption on their surface and by the formation of the so-called protein corona. The protein corona assembly, and in particular the binding of opsonins (IgG, complement components and fibrinogen) to the NPs surface, causes NPs sequestration by RES, mainly located in liver and spleen, thus reducing their half-lives in the bloodstream. The composition of the protein corona depends on the route of administration and is strongly affected by the surface properties of nanoparticles. [1, 42]

The most common method to avoid the rapid clearance of NPs is to coat their surface with polyethylene glycol (PEG), a hydrophilic surfactant that forms a tight association with water molecules, reducing opsonization and NPs elimination by RES. For this reason PEGyaltion of nanoparticle strongly increases their circulation time. [42] Alternative strategies to PEG are represented by the coating of NPs surface with cellular membranes purified by leukocytes [47] or with membranes isolated from red blood cells [48], both resulting in increased NPs retention in the bloodstream. [42]

Three generation of nanovectors have already been developed (Figure 1.7). The first generation of nanovectors consists of simple colloidal particles loaded with a therapeutic compound. They exploit passive mechanisms to deliver the drug to the target site. An example is given by doxorubicin-loaded liposomes, which take advantage of the enhanced permeability and retention (EPR) properties of tumors to reach the lesion. [49] The surface modification of first-generation nanovectors with PEG avoids immune system recognition and degradation.

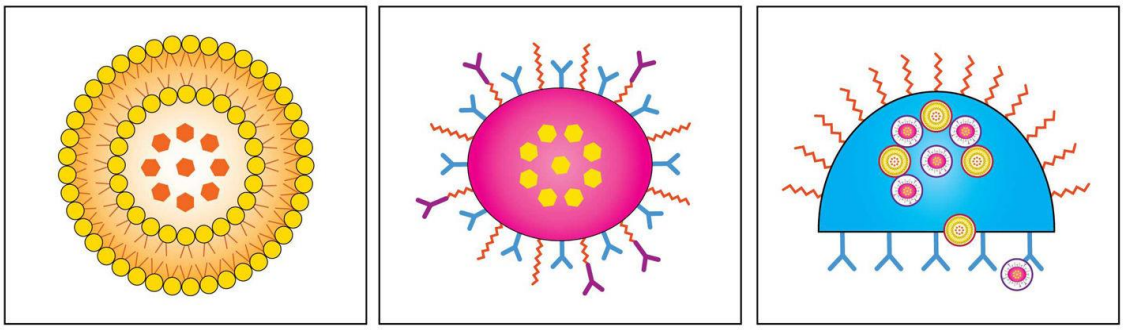

Figure 1.7. Schematic representation of first-generation (left panel), second-generation (middle panel) and third-generation (right panel) nanovectors. [49]

Second-generation nanovectors are engineered with ligands or antibodies to allow an active targeting through the binding to specific receptors. The payload release can also be modulated by pH- or enzyme-sensitive polymers, as well as by external stimuli (for instance the application of a magnetic field). Finally, third-generation nanoparticles are complex structures aiming to sequential overcoming of biological barriers and time-controlled release of multiple payloads. [49]

1.5.1 LIPID-BASED NANOPARTICLES

Lipid-based nanoparticles are mainly represented by liposomes and solid lipid nanoparticles. Both these particles have a spherical shape, dimensions up to few hundreds of nanometers and are composed of biocompatible and biodegradable lipids.

Liposomes have been the first investigated drug delivery system and doxorubicin-loaded liposomes are commercially available since 1996. [49] They are made up of one or more phospholipid bilayers, called

lamellae, which enclose an aqueous core. [50] According to their size and the number of bilayers, liposomes can be classified in multilamellar vesicles (MLV), which can be larger than 1 μm, large unilamellar vesicles (LUV) made up of a single lamella and bigger than 100 nm, and small unilamellar vesicles (SUV) composed of a single bilayer and with a size up to 100 nm. [1]

Liposomes are composed of physiological lipids, mainly sphingomyelin, phosphatididylcholine, glycerophospholipids and cholesterol; the latter reduces the bilayer fluidity and is essential for liposome stability *in vivo.* [1]

Thanks to their amphiphilic nature, liposomes can be load with both hydrophilic drugs, entrapped in the aqueous core, and lipophilic drugs, dissolved in the lipid bilayer. Encapsulation in liposomes protects drugs against degradation and enhances their circulation half-lives.

Moreover, the surface of liposomes can be easily functionalized in order to obtain a site specific targeting of the payload, thus reducing side effects. [51]

Some liposomal-based products are currently on the market, others are in various stages of clinical development. However, the majority of liposomal-based therapeutics that reaches the clinic phase is based on first-generation liposomes for the cancer therapy. These liposomes exploit the EPR effect to deliver their payload to the tumor tissue. On the contrary, liposomes functionalized for the active targeting struggle to reach the clinic; multi-functionalized liposomes are indeed more complex to produce on large scale because they require multiple synthesis steps and formulation processes, thus increasing the cost of production. [52]

Solid lipid nanoparticles (SLN) are colloidal drug delivery systems made up of lipid solid at room temperature, mainly triglycerids, fatty acids and waxes. There are many different techniques for the production of SLN, the most used include the hot or cold high pressure homogenization technique, patented by Muller and Lucks [53] and the warm microemulsion, patented by Gasco in 1993. [54]

The hot and cold homogenization techniques are already used in the pharmaceutical industry. The former is the most exploited strategy to produce SLN, the latter is used to incorporate thermolabile and hydrophilic compounds into SLN. Three models of drug incorporation into SLN have been described. According to the solid solution model, the drug is homogeneously dispersed in the lipid matrix, thus allowing a prolonged release of the therapeutic agent. This is obtained when the cold high pressure homogenization technique is used or when very lipophilic drugs are incorporated in SLN by hot high pressure homogenization. The drug-enriched shell model is obtained when a phase separation occurs

during the cooling phase and the drug concentrates in the outer layer of SLN. This configuration leads to a rapid release of the compound and could be useful for topical applications of SLN. Finally, the core-enriched incorporation occurs when the drug concentrates in the core of SLN. The diffusion rate of drug is controlled by the Fick law.[55,56]

SLN are characterized by higher entrapment efficiency and a sustained prolonged release of the payload, compared to other NPs. [1]

Nevertheless, the main limitation of SLN is related to the expulsion of the payload that can occur during storage. Indeed, during storage the solid lipid matrix could undergo a transition to a highly ordered lipid crystal, thus reducing the load capacity of SLN and increasing drug expulsion from the particle. Nanostructured lipid carriers (NLC) are second generation SLN produced to overcome this problem as well as to reduce the water content of SLN dispersion. [55, 56] NLC are characterized by a less ordered matrix compared to SLN and are classified in i) imperfect type, ii) amorphous type and iii) mixed type. Imperfect type NLC are composed of a blend of solid lipids and small amounts of oils, thus allowing drugs to clusterized in the spaces between fatty acid chains and increasing the drug payload of the particles. Amorphous type NLC are prepared by adding special lipids, such as isopropylmyristate, to the solid lipid mixture. The obtained lipid matrix is in an amorphous state and do not crystallise during storage. Finally, mixed type NLC are obtained by mixing higher amount of liquid lipids with the solid lipids. Due to the high oil content, this kind of NLC is charachterized by the formation of oil nanocompartments with higher solubility for lipophilic drugs compared to solid lipids. [55, 56]

Currently, both SLN and NLC find application in the cosmetic market and as pharmaceutical topic products. [57, 58]

1.5.2. SURFACE MODIFICATION OF NANOPARTICLES TO OVERCOME THE BBB

The treatment of several neurological disorders is still a challenge due to the presence of the BBB that hinder drug access to the CNS. The development of nanoparticle-based drug delivery system represents a promising strategy to increase drug penetration across the BBB by exploiting the transport mechanisms on the brain capillary endothelium. Therefore, the surface of NPs can be functionalized with molecules that bind receptors expressed on BECs, allowing receptor-mediated trancytosis of NPs.

Low-density lipoprotein receptor (LDL-R) is up-regulated on brain capillary endothelial cells compared to peripheral endothelium. [59-61] Together with LDL-R related protein (LRP), it is involved in apolipoprotein-E (ApoE) and B (ApoB) binding, thus allowing lipoproteins transport across the BBB.
The first evidence of ApoE-mediated transcytosis of NPs across the BBB was obtained by Kreuter et al. [62], who demonstrated that dalarginin-loaded poly(butyl cyanoacrylate) nanoparticles coated with polysorbate 80 and intravenously injected in mice were able to cross the BBB showing antinoceptive effects. It was hypothesized that polysorbate 80 acts as an anchor for the adsorption of apolipoproteins, mainly ApoE, and that polysorbate 80-coated NPs resemble endogenous lipoproteins and are taken up by receptor-mediated endocytosis by BECs. [63] Therefore the surface functionalization of NP with ApoE or peptides derived from this apolipoprotein can be exploited as strategy to increase NP access to the CNS. Indeed human serum albumin nanoparticles covalently functionalized with ApoE show enhanced BBB penetration *in vivo* compared to non-functionalized NP. [59, 64]
The specific domain involved in ApoE binding to the receptor has been localized between amino acid residues 141 and 150 (LRKLRKRLLR). This region, enriched in positively charged residues, has been successfully used by Re et al. to functionalize the surface of liposomes. [65] Results demonstrate that liposomes covalently functionalized with ApoE peptide (amino acids 141-150) are internalized by brain capillary endothelial cells and are able to cross a model of BBB, *in vitro*. [65, 66]
Moreover they can reach the brain *in vivo* after IV [67] and IP administration [68], thus representing an efficacious approach for the treatment of diseases affecting the CNS.
Noteworthy is also the role of ApoB-100 and ApoA-1 in the receptor-mediated transport of nanoparticles across the BBB. ApoB-100 binds to LDL-R and LRP, whereas ApoA-1 interaction with brain capillary endothelial cells occurs via scanvenger receptor class B type 1 (SR-B1) located at the BBB. [59]

The transferrin receptor (TfR) has also been extensively studied as a target for the drug delivery to the brain. TfR is expressed on different cell types, including endothelial cells lining brain capillaries, and it regulates the neuronal demand for iron by receptor-mediated endocytosis of transferrin. [69] Nevertheless, in order to avoid a competition between transferrin-functionalized NP and the endogenous transferrin, which is present at high concentrations in the blood, the most common approach is to decorate the surface of NP with monoclonal antibodies to epitopes of TfR distal to the Tf-binding site. [70] Different anti-Tfr mAb have been produced and used to functionalize brain targeted

PEGylated NP, included OX26 [38], 8D3 mAb [71] and R17-217 [72], providing a significant enhancement in the brain delivery of the NPs payload.

Another possibility is to decorate the surface of NPs with positively charged cell-penetrating peptides to exploit the adsorptive-mediated endocytosis mechanism. Different studies based on NPs functionalization with TAT peptide, Syn-B peptide, penetratin, as well as cationic albumin have proved the efficacy of this approach to increase NPs penetration across the BBB. [1] The main limitations of this strategy are represented by the lack of selectivity of positively charged molecules that tend to favour random tissues and organs distribution of NPs, and by the potential toxicity and immunogenicity of CPP. [27]

It is noteworthy that PEG is not only used to obtain "stealth" liposomes, thus avoiding a rapid clearance of NPs from the bloodstream, but also to act as a spacer between the NPs surface and the targeting ligand. The binding of the ligand to the PEG arm allows the former to extend beyond the PEG coating, thus supporting ligand-receptor interactions. The linkage between the spacer and the ligand should be stable, non immunogenic, should not affect the stability of the ligand and can be obtained by modifying the distal end of PEG with different reactive functional groups, such as the maleimide group. [73]

REFERENCES

1. Masserini M. Nanoparticles for brain drug delivery. *ISRN Biochem.* 2013; 2013:238428.
2. Stockwell J, Abdi N, Lu X, Maheshwari O, Taghibiglou C. Novel central nervous system drug delivery systems. *Chem Biol Drug Des.* 2014; 83:507-20.
3. Strazielle N, Ghersi-Egea JF. Efflux transporters in blood-brain interfaces of the developing brain. *Front Neurosci.* 2015; 9:21.
4. Hawkins BT, Davis TP. The blood-brain barrier/neurovascular unit in health and disease. *Pharmacol Rev.* 2005; 57:173-85.
5. Begley DJ. Delivery of therapeutic agents to the central nervous system: the problems and the possibilities. *Pharmacol Ther.* 2004; 104:29-45.
6. Ehrlich P. Ueber die beziehungen von chemischer constitution, verteilung und pharmakologischer wirkung. *Gesammelte Arbeiten zur Immunitaetsforschung*. 1904; 574.
7. Goldmann E. Vitalfarbung am zentralnervensystem. *Abhandl Konigl preuss Akad Wiss.* 1913; 1:1–60.
8. Carvey PM, Hendey B, Monahan AJ. The blood-brain barrier in neurodegenerative disease: a rhetorical perspective. *J Neurochem.* 2009; 111:291-314.
9. Chen Y, Liu L. Modern methods for delivery of drugs across the blood-brain barrier. *Adv Drug Deliv Rev.* 2012; 64:640-65.
10. Redzic Z. Molecular biology of the blood-brain and the blood-cerebrospinal fluid barriers: similarities and differences. *Fluids Barriers CNS*. 2011; 8:3.
11. Saitou M, Furuse M, Sasaki H, Schulzke D, Fromm M, Takano H, Noda T, Tsukita S: Complex phenotype of mice lacking occludin, a component of tight junction strands. *Mol Biol Cell* 2000; 11:4131-4142.
12. Saitou M, Fujimoto K, Doi Y, Itoh M, Fujimoto T, Furuse M, Takano H, Noda T, Tsukita S. Occludin-deficient embryonic stem cells can differentiate into polarized epithelial cells bearing tight junctions. *J Cell Biol.* 1998; 141:397-408.
13. Furuse M. Molecular basis of the core structure of tight junctions. *Cold Spring Harb Perspect Biol.* 2010; 2:a002907.
14. Huber JD, Egleton RD, Davis TP. Molecular physiology and pathophysiology of tight junctions in the blood-brain barrier. *Trends Neurosci.* 2001; 24:719-25.

15. Itoh M, Furuse M, Morita K, Kubota K, Saitou M, Tsukita S. Direct binding of three tight junction-associated MAGUKs, ZO-1, ZO-2, and ZO-3, with the COOH termini of claudins. *J Cell Biol.* 1999; 147:1351-63.
16. Dejana E, Lampugnani MG, Martinez-Estrada O, Bazzoni G. The molecular organization of endothelial junctions and their functional role in vascular morphogenesis and permeability. *Int J Dev Biol.* 2000; 44:743-8.
17. Ebnet K, Aurrand-Lions M, Kuhn A, Kiefer F, Butz S, Zander K, Meyer zu Brickwedde MK, Suzuki A, Imhof BA, Vestweber D. The junctional adhesion molecule (JAM) family members JAM-2 and JAM-3 associate with the cell polarity protein PAR-3: a possible role for JAMs in endothelial cell polarity. *J Cell Sci.* 2003; 116:3879-91.
18. Yamamoto T, Harada N, Kano K, Taya S, Canaani E, Matsuura Y, Mizoguchi A, Ide C, Kaibuchi K. The Ras target AF-6 interacts with ZO-1 and serves as a peripheral component of tight junctions in epithelial cells. *J Cell Biol.* 1997; 139:785-95.
19. Armulik A, Genové G, Mäe M, Nisancioglu MH, Wallgard E, Niaudet C, He L, Norlin J, Lindblom P, Strittmatter K, Johansson BR, Betsholtz C. Pericytes regulate the blood-brain barrier. *Nature.* 2010; 468:557-61
20. Hall CN, Reynell C, Gesslein B, Hamilton NB, Mishra A, Sutherland BA, O'Farrell FM, Buchan AM, Lauritzen M, Attwell D. Capillary pericytes regulate cerebral blood flow in health and disease. *Nature.* 2014; 508:55-60.
21. Dalkara T, Alarcon-Martinez L. Cerebral microvascular pericytes and neurogliovascular signaling in health and disease. *Brain Res.* 2015; 1623:3-17.
22. Satoh J, Tabunoki H, Yamamura T, Arima K, Konno H. Human astrocytes express aquaporin-1 and aquaporin-4 in vitro and in vivo. *Neuropathology*. 2007; 27:245-56.
23. Nielsen S, Nagelhus EA, Amiry-Moghaddam M, Bourque C, Agre P, Ottersen OP. Specialized membrane domains for water transport in glial cells: high-resolution immunogold cytochemistry of aquaporin-4 in rat brain. *J Neurosci.* 1997; 17:171-80.
24. Kose N, Asashima T, Muta M, Iizasa H, Sai Y, Terasaki T, Nakashima E. Altered expression of basement membrane-related molecules in rat brain pericyte, endothelial, and astrocyte cell lines after transforming growth factor-beta1 treatment. *Drug Metab Pharmacokinet*. 2007; 22:255-66.
25. Rosenberg GA. Matrix metalloproteinases and their multiple roles in neurodegenerative diseases. *Lancet Neurol.* 2009; 8:205-16.

26. Omidi Y, Barar J. Impacts of blood-brain barrier in drug delivery and targeting of brain tumors. *Bioimpacts.* 2012; 2:5-22.
27. Hervé F, Ghinea N, Scherrmann JM. CNS delivery via adsorptive transcytosis. *AAPS* J. 2008; 10:455-72.
28. Barua NU, Gill SS, Love S. Convection-enhanced drug delivery to the brain: therapeutic potential and neuropathological considerations. *Brain Pathol. 2014*; 24:117-27.
29. Kunwar S, Chang S, Westphal M, Vogelbaum M, Sampson J, Barnett G, Shaffrey M, Ram Z, Piepmeier J, Prados M, Croteau D, Pedain C, Leland P, Husain SR, Joshi BH, Puri RK; PRECISE Study Group. Phase III randomized trial of CED of IL13-PE38QQR vs Gliadel wafers for recurrent glioblastoma. *Neuro Oncol*. 2010; 12:871-81.
30. Neuwelt EA, Goldman DL, Dahlborg SA, Crossen J, Ramsey F, Roman-Goldstein S, Braziel R, Dana B. Primary CNS lymphoma treated with osmotic blood-brain barrier disruption: prolonged survival and preservation of cognitive function. *J Clin Oncol*. 1991; 9:1580-90.
31. Rapoport SI. Osmotic opening of the blood-brain barrier: principles, mechanism, and therapeutic applications. *Cell Mol Neurobiol*. 2000; 20:217-30.
32. Meairs S. Facilitation of Drug Transport across the Blood-Brain Barrier with Ultrasound and Microbubbles. *Pharmaceutics*. 2015 Aug 31;7(3):275-93.
33. Choi JJ, Selert K, Vlachos F, Wong A, Konofagou EE. Noninvasive and localized neuronal delivery using short ultrasonic pulses and microbubbles. *Proc Natl Acad Sci U S A*. 2011; 108:16539-44.
34. Dalecki D. Biological effects of microbubble-based ultrasound contrast agents. *Contrast Media in Ultrasonography - Basic Principles and Clinical Applications*. 2005;77–87
35. Gabathuler R. Approaches to transport therapeutic drugs across the blood-brain barrier to treat brain diseases. *Neurobiol Dis*. 2010; 37:48-57
36. Dhuria SV, Hanson LR, Frey WH 2nd. Intranasal delivery to the central nervous system: mechanisms and experimental considerations. *J Pharm Sci*. 2010; 99:1654-73.
37. Salameh TS, Bullock KM, Hujoel IA, Niehoff ML, Wolden-Hanson T, Kim J, Morley JE, Farr SA, Banks WA. Central Nervous System Delivery of Intranasal Insulin: Mechanisms of Uptake and Effects on Cognition. *J Alzheimers Dis*. 2015; 47:715-28.
38. Zhang Y, Pardridge WM. Blood-brain barrier targeting of BDNF improves motor function in rats with middle cerebral artery occlusion. *Brain Res*. 2006; 1111:227-9.

39. Bickel U, Yoshikawa T, Landaw EM, Faull KF, Pardridge WM. Pharmacologic effects in vivo in brain by vector-mediated peptide drug delivery. *Proc Natl Acad Sci U S A*. 1993; 90:2618-22.
40. Boado RJ, Zhang Y, Zhang Y, Wang Y, Pardridge WM. GDNF fusion protein for targeted-drug delivery across the human blood-brain barrier. *Biotechnol Bioeng*. 2008; 100:387-96.
41. Zhang X, Zhang X, Wang F. Intracellular transduction and potential of Tat PTD and its analogs: from basic drug delivery mechanism to application. *Expert Opin Drug Deliv*. 2012; 9:457-72.
42. Blanco E, Shen H, Ferrari M. Principles of nanoparticle design for overcoming biological barriers to drug delivery. *Nat Biotechnol*. 2015; 33:941-51.
43. Holmes D. The next big things are tiny. *Lancet Neurol.* 2013; 12:31-2.
44. Moghimi SM, Hunter AC, Murray JC. Nanomedicine: current status and future prospects. *FASEB J*. 2005; 19:311-30.
45. Vahidkhah K, Bagchi P. Microparticle shape effects on margination, near-wall dynamics and adhesion in a three-dimensional simulation of red blood cell suspension. *Soft Matter*. 2015; 11:2097-109.
46. Gentile F, Chiappini C, Fine D, Bhavane RC, Peluccio MS, Cheng MM, Liu X, Ferrari M, Decuzzi P. The effect of shape on the margination dynamics of non-neutrally buoyant particles in two-dimensional shear flows. *J Biomech*. 2008; 41:2312-8.
47. Parodi A, Quattrocchi N, van de Ven AL, Chiappini C, Evangelopoulos M, Martinez JO, Brown BS, Khaled SZ, Yazdi IK, Enzo MV, Isenhart L, Ferrari M, Tasciotti E. Synthetic nanoparticles functionalized with biomimetic leukocyte membranes possess cell-like functions. *Nat Nanotechnol*. 2013; 8:61-8.
48. Hu CM, Zhang L, Aryal S, Cheung C, Fang RH, Zhang L. Erythrocyte membrane-camouflaged polymeric nanoparticles as a biomimetic delivery platform. *Proc Natl Acad Sci U S A*. 2011; 108:10980-5.
49. Godin B, Driessen WH, Proneth B, Lee SY, Srinivasan S, Rumbaut R, Arap W, Pasqualini R, Ferrari M, Decuzzi P. An integrated approach for the rational design of nanovectors for biomedical imaging and therapy. *Adv Genet*. 2010; 69:31-64.
50. Hillaireau H, Couvreur P. Nanocarriers' entry into the cell: relevance to drug delivery. *Cell Mol Life Sci*. 2009; 66:2873-96.
51. Sanvicens N, Marco MP. Multifunctional nanoparticles--properties and prospects for their use in human medicine. *Trends Biotechnol*. 2008; 26:425-33.

52. Sercombe L, Veerati T, Moheimani F, Wu SY, Sood AK, Hua S. Advances and Challenges of Liposome Assisted Drug Delivery. *Front Pharmacol*. 2015; 6:286.
53. Müller RH, Lucks JS. Arzneistofftra¨ger aus festen Lipid- teilchen, Feste Lipidnanospha¨ren (SLN), European Patent No. 0605497 (1996)
54. Gasco MR. Method for producing solid lipid microspheres having a narrow size distrivution, US Patent 5 250 236 (1993).
55. Uner M, Yener G. Importance of solid lipid nanoparticles (SLN) in various administration routes and future perspectives. *Int J Nanomedicine*. 2007; 2(3):289-300.
56. Müller RH, Radtke M, Wissing SA. Nanostructured lipid matrices for improved microencapsulation of drugs. *Int J Pharm*. 2002; 242:121-8.
57. Müller RH, Shegokar R, Keck CM. 20 years of lipid nanoparticles (SLN and NLC): present state of development and industrial applications. *Curr Drug Discov Technol*. 2011; 8:207-27.
58. Pardeike J, Hommoss A, Müller RH. Lipid nanoparticles (SLN, NLC) in cosmetic and pharmaceutical dermal products. *Int J Pharm*. 2009; 366:170-84
59. Kreuter J, Hekmatara T, Dreis S, Vogel T, Gelperina S, Langer K. Covalent attachment of apolipoprotein A-I and apolipoprotein B-100 to albumin nanoparticles enables drug transport into the brain. *J Control Release*. 2007; 118:54-8.
60. Michaelis K, Hoffmann MM, Dreis S, Herbert E, Alyautdin RN, Michaelis M, Kreuter J, Langer K. Covalent linkage of apolipoprotein e to albumin nanoparticles strongly enhances drug transport into the brain. *J Pharmacol Exp Ther*. 2006; 317:1246-53.
61. Dehouck B, Fenart L, Dehouck MP, Pierce A, Torpier G, Cecchelli R. A new function for the LDL receptor: transcytosis of LDL across the blood-brain barrier. *J Cell Biol*. 1997; 138:877-89.
62. Kreuter J, Alyautdin RN, Kharkevich DA, Ivanov AA. Passage of peptides through the blood-brain barrier with colloidal polymer particles (nanoparticles). *Brain Res*. 1995; 674:171-4.
63. Kreuter J, Shamenkov D, Petrov V, Ramge P, Cychutek K, Koch-Brandt C, Alyautdin R. Apolipoprotein-mediated transport of nanoparticle-bound drugs across the blood-brain barrier. J Drug Target. 2002; 10:317-25.
64. Zensi A, Begley D, Pontikis C, Legros C, Mihoreanu L, Wagner S, Büchel C, von Briesen H, Kreuter J. Albumin nanoparticles targeted with Apo E enter the CNS by transcytosis and are delivered to neurones. *J Control Release*. 2009; 137:78-86.
65. Re F, Cambianica I, Sesana S, Salvati E, Cagnotto A, Salmona M, Couraud PO, Moghimi SM, Masserini M, Sancini G. Functionalization with ApoE-derived peptides enhances the interaction

with brain capillary endothelial cells of nanoliposomes binding amyloid-beta peptide. *J Biotechnol*. 2010; 156:341-6.

66. Re F, Cambianica I, Zona C, Sesana S, Gregori M, Rigolio R, La Ferla B, Nicotra F, Forloni G, Cagnotto A, Salmona M, Masserini M, Sancini G. Functionalization of liposomes with ApoE-derived peptides at different density affects cellular uptake and drug transport across a blood-brain barrier model. *Nanomedicine.* 2011; 7:551-9.
67. Bana L, Minniti S, Salvati E, Sesana S, Zambelli V, Cagnotto A, et al. Liposomes bi-functionalized with phosphatidic acid and an ApoE-derived peptide affect Aβ aggregation features and cross the blood-brain-barrier: implications for therapy of Alzheimer disease. *Nanomedicine* 2014; **10**:1583-90.
68. Balducci C, Mancini S, Minniti S, La Vitola P, Zotti M, Sancini G, et al. Multifunctional liposomes reduce brain β-amyloid burden and ameliorate memory impairment in Alzheimer's disease mouse models. *J Neurosci* 2014; 34:14022-31.
69. Moos T, Rosengren Nielsen T, Skjørringe T, Morgan EH. Iron trafficking inside the brain. *J Neurochem.* 2007; 103:1730-40.
70. Lajoie JM, Shusta EV. Targeting receptor-mediated transport for delivery of biologics across the blood-brain barrier. *Annu Rev Pharmacol Toxicol*. 2015; 55:613-31.
71. Zhang Y, Wang Y, Boado RJ, Pardridge WM. Lysosomal enzyme replacement of the brain with intravenous non-viral gene transfer. *Pharm Res*. 2008; 25:400-6.
72. Karatas H, Aktas Y, Gursoy-Ozdemir Y, Bodur E, Yemisci M, Caban S, Vural A, Pinarbasli O, Capan Y, Fernandez-Megia E, Novoa-Carballal R, Riguera R, Andrieux K, Couvreur P, Dalkara T. A nanomedicine transports a peptide caspase-3 inhibitor across the blood-brain barrier and provides neuroprotection. *J Neurosci*. 2009; 29:13761-9.
73. Sawant RR, Torchilin VP. Challenges in development of targeted liposomal therapeutics. *AAPS J.* 2012; 14:303-15.

Chapter II

mApoE-functionalized Solid Lipid Nanoparticles to overcome the blood brain barrier

This chapter focuses on the surface modification of solid lipid nanoparticles (SLN), prepared by warm microemulsion technique, with a syntetic peptide (mApoE) derived from the receptor binding region of human apolipoprotein E. The capability of mApoE to enhance nanoparticles penetration in the central nervous system (CNS) has already been demonstrated by using mApoE-functionalized liposomes. [1, 2, 3] Here, mApoE has been covalently conjugated to PEGylated solid lipid nanoparticles and their ability to cross the blood-brain barrier (BBB) has been evaluated. We used an *in vitro* BBB model to perform a screening among three different solid lipid nanoparticles formulations in terms of stability, internalization by brain capillary endothelial cells and permeability across the BBB model. The most promising formulation has been administered to healthy mice in order to evaluate brain accumulation of SLN following different administration routes.

2.1 METHODS

2.1.1 Preparation of SLN

SLN were prepared by Nanovector srl (Turin, Italy) by oil/water warm microemulsion technique. The microemulsion was prepared at 60-64°C by heating dynasan 116, epikuron 200, short chain alcohols, and then adding an aqueous solution of bile salts heated at the same temperature. The warm microemulsion was dispersed in cold water to obtain an aqueous dispersion of SLN. The surface of SLN was functionalized with DSPE-PEG2000-Maleimide (DPM) to perform conjugation with the peptide CWG-LRKLRKRLLR (mApoE; residues 141-150 of human apolipoprotein E) exploiting thiol-maleimide reaction, and with dipalmitoyl posphatidic acid (DPPA) as Aβ ligand, by substituting 0.4% and 10% molar percentage respectively of phosphatidylcholine (PC) with the two compounds. The peptide CWG was added at the C-term of mApoE to assess the yield of coupling reaction. Fluorescent SLN were prepared by adding the fluorescent lipophilic probes 3,3′-dioctadecyloxacarbocyanine

perchlorate (DiO, λex\λem=484\501 nm) or 1,1''-dioctadecyl-3,3,3'',3''-tetramethylindotricarbocyanine iodide (DiR, λex\λem=750\780 nm) to the oil phase of the microemulsion. Dually radiolabelled SLN were prepared using two radioactive compounds: ^{3}H-cholesteryl hexadecyl ether (^{3}H-CE) as a marker of the lipid core and ^{14}C dipalmitoyl phosphatidic acid (^{14}C –DPPA) as a marker of the Aβ ligand. SLN incorporating fluorescent probes or radioactive markers were purified by tangential ultrafiltration (repeated four times) and using Vivaflow 50 system (Sartorius, Germany) equipped with regenerated cellulose membrane 100000 MWCO.

2.1.2 Preparation and characterization of SLN functionalized with ApoE peptide

In order to obtain brain targeted SLN, fluorescent and radiolabelled SLN were incubated with mApoE overnight at 4°C, protected from light. The final mApoE:DSPE-PEG2000-Mal molar ratio was 1:1. After the incubation, the reaction mixture was purified by tangential ultrafiltration to remove unbound peptide by using a 300 KDa membrane. The yield of coupling reaction between SLN and mApoE was assessed by fluorescence spectroscopy of tryptophan residue at the C-terminal of mApoE, as described by Re et al. [3] As a control, non-functionalized SLN (SLN-cys) were prepared by incubation with cysteine in order to block maleimide reactive site. SLN were characterized in terms of dimension, ζ-potential and polydispersity index by means of Dynamic Light Scattering (DLS) analysis.

2.1.3 Culture of hCMEC/D3 cells

Human cerebral microvascular endothelial cells (hCMEC/D3) were obtained from Institut Cochin (INSERM, Paris, France). Cells at passages between 27 and 37 were grown on tissue culture flasks, covered with 0.1 mg/ml rat tail collagen type 1, in EBM-2 medium supplemented with 5% fetal bovine serum (FBS), 1% Penicillin-Streptomycin, 1.4 μM hydrocortisone, 5 μg/ml ascorbic acid, 1/100 chemically defined lipid concentrate, 10 mM HEPES and 1 ng/ml basic FGF. Cells were seeded at a density of 24,000 – 33,000 cells/cm^2 and cultured at 37°C, 5% CO_2. For permeability assays cells were seeded on 12-well Transwell® inserts coated with rat tail collagen type 1; cell culture medium was changed every 2 days. For uptake studies by confocal microscopy, hCMEC/D3 were grown on 25 mm glass coverslips precoated with collagen; confluent hCMEC/D3 monolayers were obtained typically by day 3. For flow citometry analysis, cells were cultured on type 1 collagen-coated 12-well plates; confluent hCMEC/D3 monolayers were obtained typically by day 3.

2.1.4 Citotoxicity Assay

Cell viability after incubation with SLN was assessed by means of PrestoBlue assay (Invitrogen). hCMEC/D3 were seeded in 24-wells plates. Once confluence was reached, cells were incubated with SLN-cys or SLN-mApoE at the final lipid concentrations of 0.05 mg/ml, 0.1 mg/ml, 0.5 mg/ml or 1 mg/ml for up to 24 hours, at 37°C, 5% CO_2. At the end of the incubation period, culture medium was removed, PrestoBlue solution was added to each well and the 24-well plates were incubated at 37°C. Absorbance was measured at different time points until a plateau was reached. Values were measured as OD readings at 570/600 nm using FLUOStar Omega Multidetection Microplate reader (BMG LABTECH).

2.1.5 Flow citometry

In order to quantitatively evaluate the cellular uptake of SLN, hCMEC/D3 were incubated with DiO-labelled SLN-cys or SLN-mApoE at the final total lipid concentration of 0.1 mg/ml for up to 5 hours at 37°C. At different time points, cells were prepared for fluorescence-activated cell sorting (FACS) analysis. Data corresponding to 20,000 events in a user-determined area were collected for every experimental condition. Experiments were performed in triplicate, n=3. Samples were analysed using DIVA software on a FACSCanto I (BD Biosciences, San Jose, California).

2.1.6 Immunofluorescence

Qualitative data about cellular uptake of SLN and their intracellular distribution were acquired using confocal laser scanning microscopy (CLSM). Cells were incubated with DiO-labelled SLN (0.1 mg/ml of total lipids) for 3 hours and overnight at 37°C, and fixed in 10% formalin solution. Immunofluorescence technique was used to stain different intracellular compartments. The following antibodies were used: mouse anti-Calreticulin (1:200 in BSA 1%), mouse anti-EEA1 (1:250 in GDB 1X), mouse anti-GM130 (1:700 in GDB 1X), rabbit anti-LAMP1 (1:200 in BSA 1%), rabbit anti-Niemann-Pick C1 (1:200 in BSA 1%), rabbit anti-Rab11 (1:200 in BSA 1%), Alexa Fluor 568 goat anti-mouse (1:200), Alexa Fluor 568 goat anti-rabbit (1:600). Briefly, cells were permeabilized with gelatin dilution buffer (GDB 1X) or with 3% BSA + 0.5% Triton X-100 for 1 hour at room temperature, and incubated with the primary antibody in the appropriate blocking buffer for 3 hours at room temperature. Then cells were incubated with the secondary antibody for 1 hour at room temperature. Actin filaments were stained using a solution of 1% Phalloidin in PBS, while nuclear

staining was performed using DAPI (1:5000) in PBS. Samples were mounted on microscope slides using ProLong® Gold antifade reagent (Life Technologies).

2.1.7 Pathways involved in cellular uptake of SLN-mApoE

To evaluate the mechanisms involved in hCMEC/D3 uptake of SLN-mApoE, cells were pre-incubated with the following endocytosis inhibitors: amiloride (100 µM), filipine (3µM) or chlorpromazine (30 µM). After 30 minutes, the medium was removed and fresh medium containing DiO-labelled SLN-mApoE (0,1 mg/ml of total lipids) and inhibitors was added and incubated for 3 hours. Subsequently cells were prepared for FACS analysis. As control, cells incubated with SLN-mApoE without any inhibitor were used.

2.1.8 Endothelial permeability of radiolabelled SLN

In *vitro* evaluation of SLN passage across a model of BBB was performed by means of transwell system. hCMEC/D3 were seeded in 12-well transwell inserts (polyester membrane; 0.4 µm pore size) coated with rat tail collagen type 1 at a density of 62,500 cells/cm^2. Experiments were usually performed 14 days after seeding, when a constant transendothelial electrical resistance (TEER) value, measured using an EVOM Endohm chamber (World Precision Instruments), was obtained. Transwell system allows the formation of two compartment, an upper one (0.5 ml), representative of the blood and a lower one representative of the brain (1 ml) (Figure 2.1). Dually radiolabelled SLN-cys or SLN-mApoE at the final total lipid concentration of 0.1 mg/ml in PBS were incubated in the upper chamber. Samples were taken from the lower compartment at different time points (60 and 180 minutes) and the radioactivity was measured using a Tri-Carb 2200 CA Liquid Scintillation Analyzer (Packard). Transendothelial permeability (EP) was calculated as previously described [3,4], according to the following equation:

$$EP = \frac{amount\ of\ LIP\ in\ the\ bottom\ compartment}{concentration\ of\ LIP\ in\ the\ apical\ compartment} * \frac{1}{\Delta t} * \frac{1}{surface\ area}$$

where the amount (dpm)/concentration (dpm/ml) of LIP was determined by lipid-associated radioactivity; Δt = time (min); surface area = area of transwell insert filter (cm^2).

The efflux of the hydrophilic marker ^{14}C-sucrose (200 µM) added in the upper chamber was measured to evaluate the paracellular permeability of hCMEC/D3 monolayer.

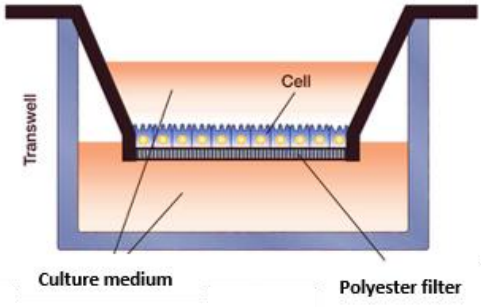

Figure 2.1 Schematic representation of the transwell system

2.1.9 In vivo SLN administration

SLN biodistribution was evaluated by means of FMT1500^{TM} Fluorescence Molecular Tomography system (Perkin Elmer). This small-animal imaging system is equipped with a near-infrared 750 nm channel and it provides tomographic and quantitative data about the biodistribution of a fluorescence signal.

Intraperitoneal (IP) administration, intravenous (IV) injection and intratracheal (IT) instillation were performed on mice kept under anaesthesia during the whole administration and fluorescence detection procedure (n=10 per group). For each treatment, SLN loaded with 40 µM DiR at the final total lipid concentration of 10 mg/ml were used. Five animals per group were treated with 50 µl of SLN-cys, the other five mice with 50 µl of SLN-mApoE. IT instillation was performed using a MicroSprayer Aerosolizer system (Penn Century, USA), while for the intravenous administration SLN were injected in the tail vein of mice. After SLN administration, anesthetised mice were placed into the imaging cassette inside the chamber of the instrument. The total amount (in picomoles) of fluorophore in a selected tridimensional region of interest (ROI) was calculated by the TrueQuant software using previously generated standards of the appropriate dye. [5] ROI were individually selected in a blind manner by an operator unaware of the experimental origin of the specimens in order to eliminate any operator bias. Every mouse was scanned immediately after the treatment, then 1h, 3h and 24 hours after SLN administration. A group of 6 animals (2 mice for each administration route) was treated with 50 µl of DiR and used as control. During the whole experiment no changes in animals weights and behaviour were found.

2.1.10 Bronchoalveolar lavage fluid analysis

24 hours after IT instillation, 5 mice treated with 50 µl of isotonic saline solution (sham) and 5 mice treated with 50 µl of SLN-mApoE were euthanized by cervical dislocation and bronchoalveolar lavage (BAL) fluid was collected and processed, as described by Mantecca et al. [6] Briefly, the trachea was exposed, cannulated and three in-and-out washes with 0.6 ml of saline isotonic solution were performed. The collected BAL fluid was centrifuged at 1500 × *g* for 15 min at 4°C. Supernatants were stored for biochemical analysis, while pellets were collected for cell counts.

Cell counts. In order to perform a differential count of alveolar macrophages (AMs), polymorphonuclear leukocytes (PMNs) and lymphocytes, pellets collected from BAL fluids were resuspended in 0.5 ml of Dulbecco's Modified Eagle Medium (DMEM). A cell aliquot (240,000 cells/0.3 ml) was smeared on a slide by centrifugation at 40 × *g* for 7 min using Cytofuge 2 (StatSpin, USA). [6] The smears were stained using Diff Quick (Medion Diagnostic) according to the manufacturer's protocol.

Cytokine analysis. The level of pro-inflammatory cytokine IL-1β was investigated in cell-free BAL fluid supernatants from both sham and SLN-treated mice. Analysis was performed using a DuoSet ELISA kit for IL-1β (R&D Systems, Minneapolis, MN - USA) according to the manufacturer's protocol. Optical density was measured at 450 nm.

2.1.11 OTHER TESTED SLN FORMULATIONS

2.1.11.1 Preparation of SLN-CLABP and SLN-GLYST

SLN-CLABP and SLN-GLYST were prepared by Nanovector srl by warm microemulsion technique, as described in chapter 2.1.1. To obtain SLN-CLABP, the microemulsion was prepared at 60-64°C by heating a mixture of cholesterol esters (confidential information), epikuron 200 and alcohols and then adding an aqueous solution of bile salt and PEG-40-stearate heated at the same temperature. The surface of SLN-CLABP was functionalized by substituting 1-2% and 10% molar percentage respectively of PC with DSPE-PEG-Maleimide and DPPA. Fluorescent SLN-CLABP were prepared by incorporating the fluorescent lipophilic dye DiO in the lipid matrix. Radiolabeled SLN-CLABP were prepared by using the radioactive compound ^{3}H cholesteryl hexadecyl ether.

To produce SLN-GLYST the microemulsion was prepared at 60°C by using a mixture of glyceryl stearate citrate and glycerol monostearate as lipid matrix (confidential information). SLN-GLYST were functionalized with DSPE-PEG-Maleimide by substituting 0.6% molar percentage of PC. Fluorescent SLN-GLYST were prepared by incorporating the lipophilic cyanine dye DiO in the lipid matrix, whereas radiolabelled SLN-GLYST were prepared by using ^{3}H-CE as a marker of the lipid core.

SLN-CLABP and SLN-GLYST were coupled with mApoE performing conjugation reaction and purification procedure in the same conditions described in chapter 2.1.1. After purification, SLN-CLABP were sterilized by filtration through 0.2 μm membrane.

2.1.11.2 Cellular uptake of DiO-labelled SLN-CLABP and SLN-GLYST

The cellular uptake of SLN-CLABP and SLN-GLYST by hCMEC/D3 was evaluated by means of CLSM using DiO-labelled formulations. hCMEC/D3 were incubated with SLN-CLABP, SLN-CLABP-mApoE, SLN-GLYST or SLN-GLYST-mApoE (0.1 mg/ml of total lipids) overnight at 37°C, and fixed in 10% formalin solution. Nuclei were stained using DAPI (1:5000) in PBS. The samples were mounted on microscope slides using ProLong® Gold antifade reagent.

2.1.11.3 Endothelial permeability of ^{3}H-labelled CLABP-SLN and CORIS-SLN across hCMEC/D3

hCMEC/D3, seeded in 12-well transwell inserts (as reported in chapter 2.1.1), were incubated with 0.1 mg/ml of total lipids of ^{3}H-labelled SLN-CLABP, SLN-CLABP-mApoE, SLN-GLYST or SLN-GLYST-mApoE for up to 3 hours at 37°C. The endothelial permeability was calculated as described in chapter 2.1.8.

2.2 RESULTS

2.2.1 Physicochemical characterization of SLN

SLN were characterized by Nanovector srl in terms of average diameter and size distribution before (BW=before washing) and after washing (AW) performed by tangential ultrafiltration with RC 100KD membrane.

The physicochemical characterization of fluorescent SLN functionalized with DPPA and DSPE-PEG-Maleimide is reported in table 2.1.

Table 2.1 Charachterization of DiO- and DiR-loaded SLN

SLN	Dye	DPPA	DPM	Av. Diam. (nm)	P.I.	Tripalmitin (rec.%) HPLC	PC (rec.%) HPLC
Dio-DPPA-MAL BW	Dio	10%molPC	0.4%molPC	120.0	0.235	86%	105%
Dio-DPPA-MAL AW			(DPM20)	103.7	0.236	85%	83%
Dir-DPPA-MAL BW	Dir	10%molPC	0.4%molPC	100.3	0.259	93%	111%
Dir-DPPA-MAL AW			(DPM20)	99.68	0.279	92%	85%

The physicochemical parameters of fluorescent SLN were determined for each step of the conjugation procedure, as reported in figure 2.2. The coupling efficiency between SLN and mApoE, assessed by fluorescence spectroscopy of tryptophan residue, was >90%.

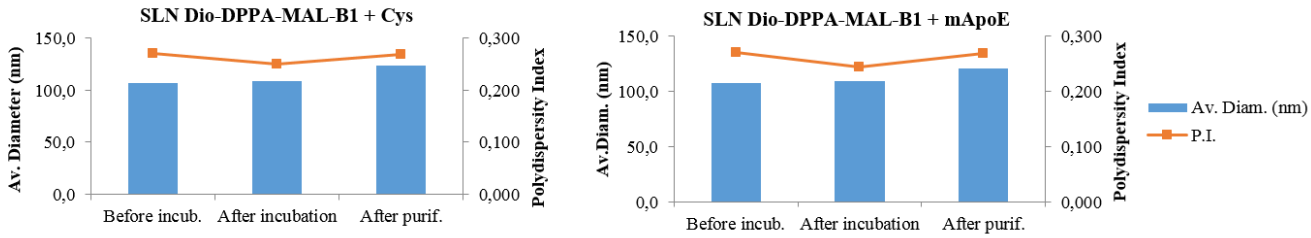

Figure 2.2. Physicochemical characterization of SLN-cys and SLN-mApoE**.** Average diameter and polydispersity index of SLN were monitored before and after the coupling procedure.

A slightly increase in the average diameter of SLN was observed after the purification procedure for both SLN conjugated with mApoE and SLN-cys. Purified SLN-cys had a mean diameter 121.5±2.1 nm and a ζ-potential of -62.4±2.5 mV. SLN-mApoE had a mean diameter 119.7±2.5 nm and a ζ-potential of -54.3±2.1 mV.

2.2.2 Cytotoxicity

Cell toxicity induced by incubation with SLN was evaluated by means of PrestoBlue assay. hCMEC/D3 were incubated with increasing concentrations of SLN-cys or SLN-mApoE and cell viability was assessed 24h after the incubation. No reductions of cell viability were observed neither in presence of SLN-cys nor of SLN-mApoE, suggesting that these SLN formulations did not exert any toxic effect on the *in vitro* BBB model (Figure 2.3).

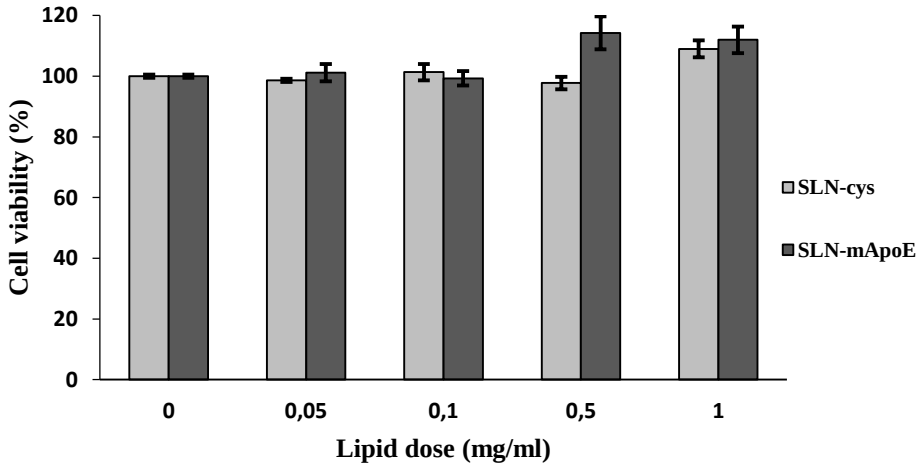

Figure 2.3. Citotoxicity of SLN. hCMEC/D3 viability did not significantly change after incubation with increasing concentrations of SLN-cys or SLN-mApoE. Each value is the mean of three independent experiments; SEM are presented as bars.

2.2.3 Cellular uptake of fluorescent SLN

Time-dependent uptake of SLN was quantitatively evaluated by FACS analysis. hCMEC/D3 were incubated with 0.1 mg/ml of DiO-labelled SLN-mApoE or SLN-cys and the cell associated fluorescence was measured at different time point. The cell associated fluorescence increased over

time, both for SLN-mApoE and SLN-cys, but it was about two-fold higher in presence of SLN-mApoE compared to SLN-cys, at each considered time point (Figure 2.4.).

As expected, the surface functionalization of SLN with ApoE peptide plays a major role in promoting their cellular uptake.

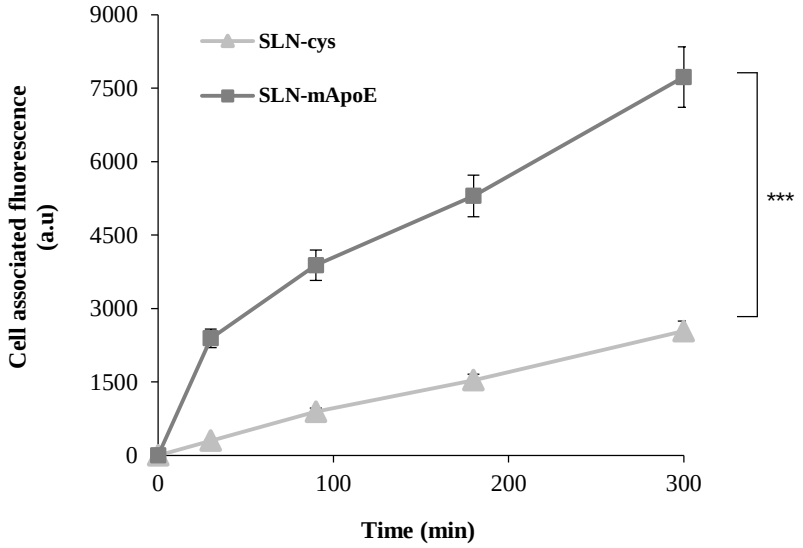

Figure 2.4. Time dependent uptake of DiO-labelled SLN in hCMEC/D3. Cells were incubated with SLN-cys or SLN-mApoE for 30, 90, 180, 300 minutes and the cell associated fluorescence was detected and quantified by FACS analysis. The cell associated fluorescence of SLN-mApoE (heavy grey line) was higher compared to values obtained with SLN-cys (light grey line) at each time point. Each value is the mean of three independent experiments; the SDs of means are presented as bars. *** $p<0.001$ by Student's *t* test.

The difference between SLN-mApoE and SLN-cys internalization was confirmed by CLSM analysis. After overnight incubation with SLN-mApoE, green spots were observed below the plasma membrane and at the perinuclear region of hCMEC/D3, while in presence of SLN-cys a smaller amount of fluorescence was detected into cells (Figure 2.5 A-B). In order to investigate the intracellular distribution of SLN-mApoE, endosomes and lysosomes as well as Niemann-Pick C1-positive vesicles and Rab11 vesicles were stained. SLN-mApoE did not co-localize with any of these compartments, neither after 3 hours of incubation (images not shown) nor after overnight incubation (Figure 2.5 C-F). The same intracellular distribution was observed in presence of SLN-cys (data not shown).

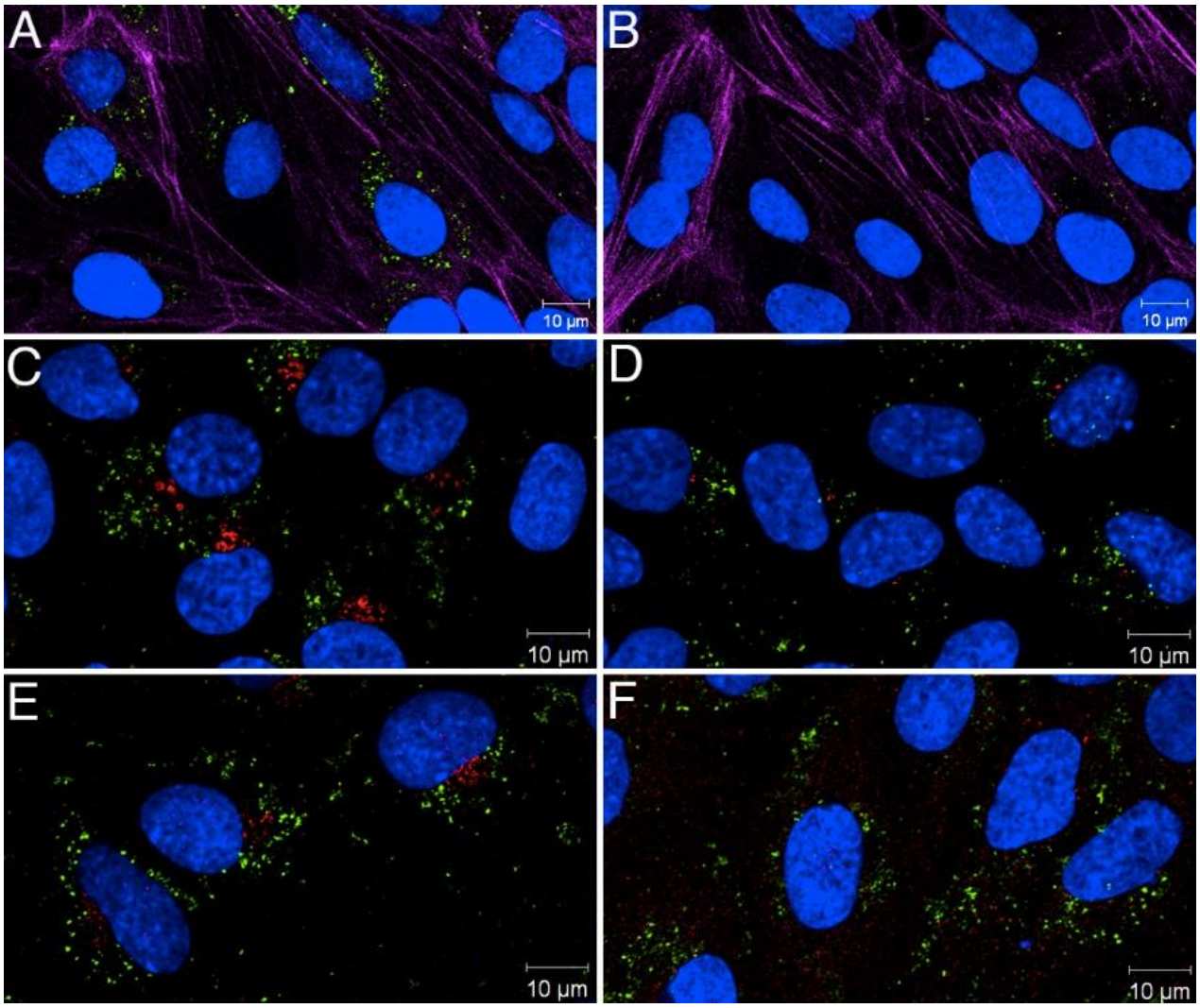

Figure 2.5. Cellular uptake and intracellular distribution of SLN in hCMEC/D3. Cells were incubated overnight with DiO-labelled SLN (green) and the fluorescent signal was visualized by CSLM. SLN-mApo (A) showed an increased internalization in hCMEC/D3 compared to SLN-cys (B). Intracellular localization of SLN-mApo was evaluated by cytoplasmic organelles staining (red); SLN-mApo did not co-localize with any intracellular compartment, neither with the acid organelles of the cell, namely early endosomes (C) and late endosomes/lysosomes, (D) nor with recycling vesicles, namely Rab11 (E) and Niemann-Pick C1 positive (F) vesicles. Actin filaments were stained with Phalloidin 633nm (magenta), while nuclei were counterstained with DAPI (blue). Bars: 10 µm.

In order to explore the internalization pathways of SLN-mApoE in hCMEC/D3, the effect of the following transcytosis chemical inhibitors was evaluated: chlorpromazine to inhibit clathrin-coated pits development, filipine to hinder caveolae/lipid rafts transport through cholesterol-depletion, and the macropinocytosis inhibitor amiloride to act on Na+/H+ exchange. FACS analysis indicated that co-

incubation of SLN-mApoE with chlorpromazine resulted in a 51% reduction of cell-associated fluorescence compared to control cells, while filipine and amiloride produced, respectively, a reduction of 23% and 12% of SLN-mApoE uptake compared to control. The decrease of cell–associated fluorescent signal was statistically significant ($p<0.01$) for all the chemical inhibitors tested.

2.2.4 SLN permeability across hCMEC/D3 monolayer

The ability of SLN to cross the in *vitro* hCMEC/D3 BBB model was assessed using dually radiolabelled formulations. In order to exclude alterations of the tight junction properties triggered by cell incubation with SLN, the paracellular permeability of ^{14}C-sucrose was evaluated before each experiment; the EP value of ^{14}C-sucrose was about 1.5×10^{-3} cm/min both in presence and in absence of SLN, according to data already published for this BBB model. [7] As shown in Figure 2.6, the functionalization of SLN with ApoE peptide was related to a higher transendothelial permeability across hCMEC/D3 monolayer compared to the non-functionalized formulation. The EP value for ^{14}C-DPPA was of $5.7\pm0.3 \times 10^{-5}$ cm/min for SLN-mApoE, while the EP value of SLN-mApoE calculated as ^{3}H-CE was of $6.9\pm0.4 \times 10^{-5}$ cm/min. EP values obtained with the two radiotracers were equivalent for the same SLN formulation, and about 6-fold higher by using SLN-mApoE compared to SLN-cys. These results suggest that, at least at the tested dose, SLN are able to cross intact the cell monolayer.

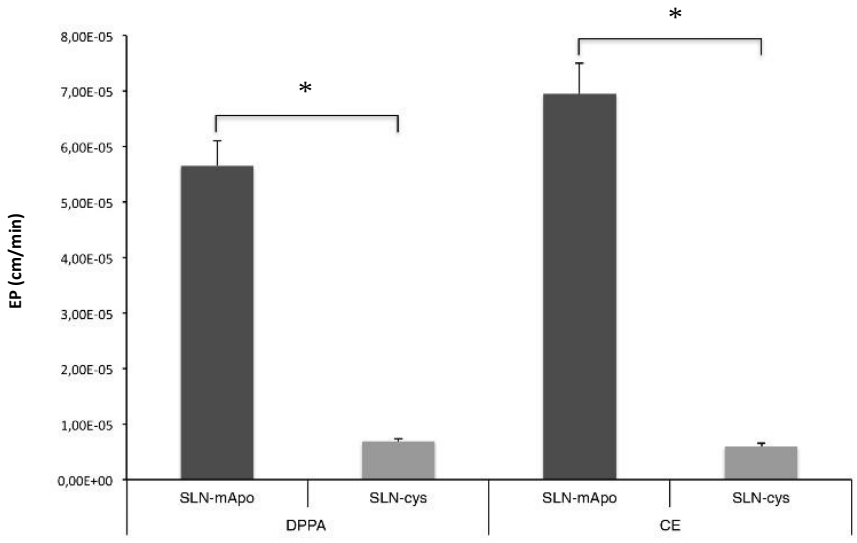

Figure 2.6. Transport of dually radiolabelled SLN across hCMEC/D3 monolayer. Cells were incubated with SLN-cys or SLN-mApoE at the final total lipid concentration of 0.1 mg/ml. The transendothelial permeability of SLN was calculated

and expressed as EP (cm/min). Functionalization of SLN with mApo (heavy grey bars) is related to higher EP values compared to SLN-cys (light grey bars). Each value is the mean of three independent experiments. The SDs of means are presented as bars. * = p< 0.01 by Student's *t* test

2.2.5 In vivo SLN biodistribution

In order to evaluate the capability of mApoE functionalization to increase SLN brain targeting, 50 µl of DiR-labelled SLN-mApoE or SLN-cys were administered by IV injection or IT instillation to healthy mice. Three hours after IT instillation, the fluorescence signal displayed by SLN-mApoE in the selected ROI, drawn considering the whole mice cranial volume, was about three-fold higher compared to the fluorescence displayed by SLN-cys. Mice were monitored until 24 hours after IT. At this time, SLN-mApoE fluorescence was still detectable in the brain (1.7% of the injected dose) (Table 2.2).

Table 2.2. Amount of DiR fluorescence in the brain

		SLN-mApoE (n=5)				**SLN-cys (n=5)**			
		ROI[a] (mm^3)	**DiR (pmol)**	± SEM (pmol)	**% of inj. dose**	ROI (mm^3)	**DiR (pmol)**	± SEM (pmol)	**% of inj. dose**
IT[b]	**3h**	1342.51	**90.45**	36.9	**4.52**	1338.80	**27.71**	3.39	**1.38**
	24h	1335.54	**35.04**	15.96	**1.75**	1346.02	**7.24**	3.08	**0.36**
IV[c]	**3h**	1340.12	**2.97**	2.39	**0.15**	1346.12	**13.35**	4.66	**0.67**
	24h	1337.37	**1.31**	0.95	**0.06**	1355.61	**3.36**	1.73	**0.17**

(*) p<0.01; (a) Region of interest; (b) Intratracheal instillation; (c) Intravenous injection

Three hours after the administration, the brain fluorescence displayed by SLN-mApoE administered by IT injection was significantly higher compared to the results obtained by IV injection, both 3h and 24h after the treatment.

On the contrary, the fluorescence displayed by IP administered SLN-mApoE was mainly limited at the abdominal cavity and no detectable signal was measured in the brain at any time (Figure 2.7).

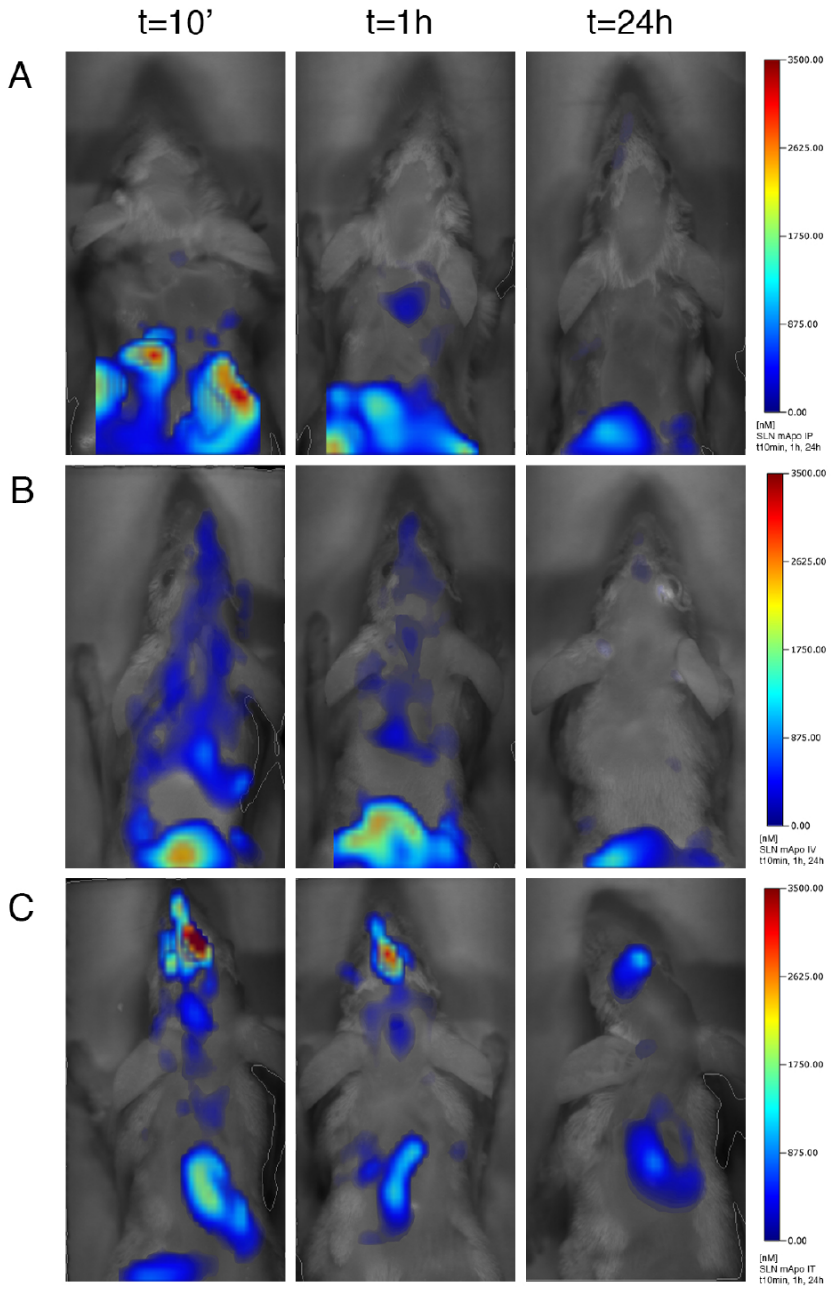

Figure 2.7. In vivo biodistribution of fluorescent SLN. Mice were treated with DiR-labelled SLN-mApoE at the final total lipid concentration of 0.1 mg/ml. Images were acquired at 10 minutes, 1 hour and 24 hours after treatment using FMT1500. A more efficient delivery of SLN-mApoE to the brain was obtained by means of IT instillation (panel C) compared to IP (panel A) and IV (panel B) administrations. (IP, intraperitoneal injection; IV, intravenous injection; IT, intratracheal instillation)

IT instillation of SLN-mApoE enhanced their brain targeting and prolonged their retention in the brain up to 24 hours after the administration. To exclude DiR release from SLN, a group of mice (2 mice for each administration route) was treated with the free fluorophore by IT, IV or IP administration. After IP and IV injections, no detectable amount of fluorescence was measured in the brain, while the percentage of DiR in the brain 24 after IT instillation (measured as % of the injected dose) was lower than 0.2%.

2.2.6 Bronchoalveolar lavage fluid analysis

The feasibility of IT instillation as a route for SLN administration was investigated by means of BAL fluid analysis, in order to exclude inflammatory reactions triggered by SLN-mApoE persistence in the lungs. The differential count of the immune cells found in the BAL fluid proved that 24 hours after IT instillation no significant differences in the percentage of AMs and PMNs (99% neutrophils) were found between sham and SLN-mApoE-treated mice. Moreover, the concentration of the cytokine IL-1β did not enhance in treated mice compared to sham (Table 2.3).

Table 2.3. BALf analysis

	sham (n=5)		**SLN-mApoE (n=5)**	
	mean	**± SEM**	**mean**	**± SEM**
AMs[a] (%)	82.58	14.14	64.25	11.86
PMNs[b] (%)	17.41	14.14	35.74	11.86
IL-1β[c] (pg/ml)	25.23	8.99	26.94	14.44

(a) Alveolar macrophages; (b) Polymorphonuclear leukocytes; (c) Interleukin-1β

2.3 SLN-CLABP AND SLN-GLYST: RESULTS

2.3.1 Physicochemical characterization

SLN-CLABP and SLN-GLYST were characterized in terms of composition, average size and polydispersity index before (BW) and after washing (AW). Results are reported in table 2.4.

Table 2.4. Charachterization of SLN-CLABP and SLN-GLYST

	Fluo. dye	**DPPA**	**DPM**	**Av. Diam. (nm)**	**P.I.**	**Chol. ester (rec.%) HPLC**	**PC (rec.%) HPLC**
SLN-CLABP-MAL BW	--	10%mol PC	2%mol PC	112.7	0.193	96%	108%
SLN-CLABP-MAL AW				114.6	0.212	100%	102%
DiO-SLN-CALBP-MAL BW	Dio	10%mol PC	2%mol PC	134.7	0.224	88%	104%
DiO-SLN-CALBP-MAL AW				137.7	0.250	94%	94%
SLN-GLYST BW	--	--	--	54.37	0.124	NA[a]	NA
SLN-GLYST A6W				56.07	0.163	NA	NA
DiO-SLN-GLYST-MAL BW	DiO	--	0.6%mol PC	57.72	0.116	NA	NA
DiO-SLN-GLYST-MAL A4W				57.76	0.158	NA	NA

(a) not available, confidential information

The physicochemical parameters of SLN-CLABP and SLN-GLYST were determined for each step of the conjugation procedure with mApoE and no changes in the average diameter of the functionalized formulations were observed compared to the non-functionalized ones. The ζ-potential value was of -29.1±1.2 mV for SLN-CLABP and of -32.5±1.3 mV for SLN-GLYST. The stability of SLN-CLABP-mApoE and SLN-GLYST-mApoE was assessed following incubation in hCMEC/D3 culture medium at 37°C. The average size of both formulations slightly increased after o/n incubation in medium.

2.3.2 Uptake of fluorescent SLN-CLABP and SLN-GLYST

After overnight incubation with the different SLN formulations, the fluorescence within hCMEC/D3 was detected by means of CLSM. SLN-CLABP-mApoE were found in the cytosol (Figure 2.8, A).

On the contrary, a weak fluorescence, almost undetectable, was observed in cells incubated with SLN-CLABP (data not shown). Concerning SLN-GLYST and SLN-GLYST-mApoE, some bright green spots were found below the plasma membrane, but the most of fluorescence was associated to SLN aggregates outside of the cells (Figure 2.8, B). The functionalization of SLN-GLYST with ApoE peptide did not increase their cellular uptake.

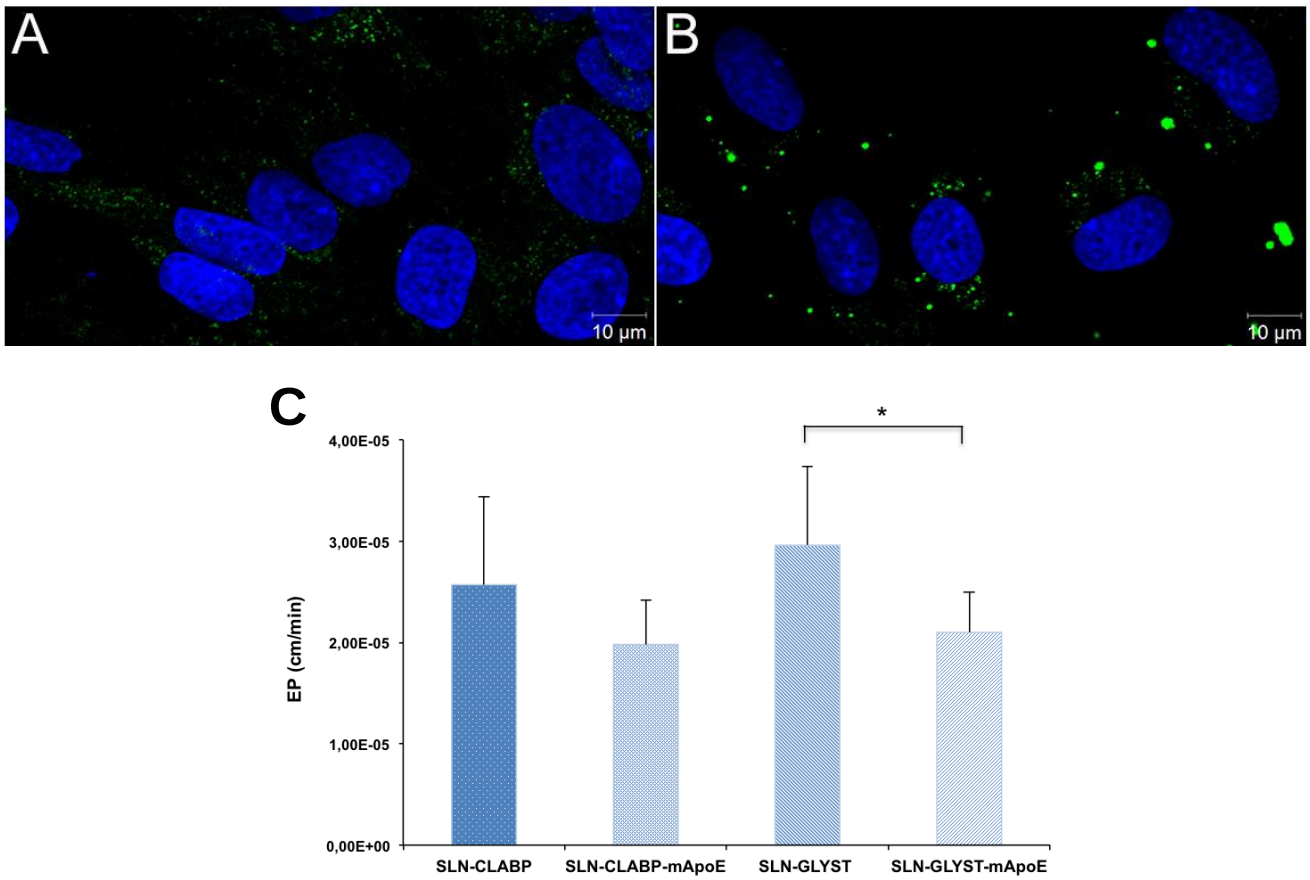

Figure 2.8. Cellular uptake and endothelial permeability of SLN-CLABP and SLN-GLYST. (A-B) hCMEC/D3 were incubated o/n with DiO-labelled SLN-CLABP-mApoE or SLN-GLYST-mApoE. SLN-CLABP-mApoE were taken up by the cells and distributed in the cytosol (A), while SLN-GLYST-mApoE aggregates were observed outside of the cell (B). (C) The functionalization of ^{3}H-labelled SLN-CLABP and SLN-GLYST with mApoE did not enhance the flux across the BBB model. Experiments were performed in triplicate; the SDs of means are presented as bars. * $p<0.05$ by Student *t* test

2.3.3 Endothelial permeability across hCMEC/D3 monolayer

The EP of SLN-CLABP and SLN-GLYST across the *in vitro* blood-brain barrier model was measured using ^{3}H-labelled formulations. As shown in Figure 2.8, panel C, the EP values of ^{3}H-CE were similar for both SLN-CORIS and SLN-GLYST (2.6±0.9 × 10^{-5} vs 2.9±0.8 × 10^{-5} cm/min, respectively). The surface modification of nanoparticles with ApoE peptide did not enhance their EP (SLN-CLABP-mApoE = 1.9±0.8 × 10^{-5} cm/min; SLN-GLYST-mApoE = 2.1±0.4 × 10^{-5} cm/min) and SLN-GLYST-mApoE endothelial permeability was significantly reduced in comparison to non-functionalised SLN-GLYST.

2.4 DISCUSSION

Solid lipid nanoparticles are colloidal systems with usual dimensions in the range of 40-200 nm made of biocompatible and biodegradable lipids. They have been extensively investigated for drug delivery. The warm microemulsion technique was patented by Gasco at the beginning of 1990s [8] and allows the preparation of SLN with modulable designed surface characteristics: this method is based on the preparation of a warm oil/water microemulsion, where the oily phase is represented by the melted lipid or a mixture thereof, which constitutes the matrix of the particle. The oily phase is maintained at a temperature above its melting point and rapidly cooled by dilution in cold water to force the solidification of the oil droplets and the formation of SLN.

To improve the half-life of SLN, avoiding opsonisation [9], and to functionalize SLN with ApoE peptide, the surface of SLN has been modified by incorporating DSPE-PEG2000-Mal during the production process. The functionalization with the ApoE peptide was obtained by conjugation of mApoE to the surface of SLN exploiting the reaction between the thiol group at one terminal end of mApoE and the maleimide located on the surface of SLN. The covalent conjugation was performed in the pH range 6.5-7.5 in conditions that maintain the biological properties of the peptide. Using this technique, three SLN formulations, which differ in the composition of the lipid matrix, were prepared by Nanovector srl.

The *in vitro* experiments were carried out using a transwell system made by hCMEC/D3 as blood-brain barrier model. [1] It is worth noting that the composition of the lipid matrix strongly affects SLN uptake and ability to cross the hCMEC/D3 monolayer. Indeed, the surface functionalization of SLN-CLABP

and SLN-GLYST with ApoE peptide did not enhance their endothelial permeability, which was much lower respect to the values obtained using the SLN-mApoE formulation described in chapter 2.1.1. Moreover, some aggregates of SLN-GLYST (both with and without functionalization with mApoE) were observed by CLSM. For these reasons, we did not perform further *in vivo* studies using SLN-CLABP and SLN-GLYST formulations and the discussion will focus on results obtained using SLN-cys and SLN-mApoE.

The here obtained results show that mApoE functionalization significantly improve SLN internalization in hCMEC/D3, according to published findings obtained by using mApoE-functionalized liposomes. [1, 10] As hypothesized by Bana et al., SLN-mApoE could exploit a receptor-mediated endocytosis mechanism to be taken up by brain capillary endothelial cells. [1] The involvement of a receptor-mediated pathway for SLN-mApoE cellular uptake is also supported by the finding that hCMEC/d3 incubation with chlorpromazine, which inhibits clathrin-coated pits development, significantly reduces the uptake of SLN-mApoE respect to control cells. It is worth noting that clathrin-mediated endocytosis is not the only pathway involved in SLN-mApoE internalization. There are also evidences of a partial involvement of caveolae-mediated endocytosis (filipine reduced SLN-mApoE uptake of 23%), which are enriched in brain capillary endothelial cells [11] and of clathrin- and caveolae-indipendent mechanisms.

Confocal microscopy data indicate that SLN-mApo do not co-localize neither with early and late endosomes nor with lysosomes thus prolonging SLN intracellular bioavailability within hCMEC/D3 cells, as also suggested for LIP with the same surface functionalization. [10] Indeed, in analogy with LDL, NPs functionalized with ApoE-derived peptides (corresponding to the receptor binding domain of ApoE) could be transported across the BBB by transcytosis, bypassing the lysosomal degradation.[11,12]

Permeability experiments across the *in vitro* BBB model, carried out by radiochemical technique, showed that the surface functionalization of SLN with mApoE strongly enhanced SLN flux across the cell monolayer. Moreover, the ratio between the two radiotracers was maintained both in the upper chamber and in the lower compartment of the transwell system, suggesting that SLN-mApoE cross intact the cell monolayer and confirming the results previously obtained using LIP with the same surface functionalization. [1]

In vivo experiments, carried out in healthy mice using the FMT1500 system, demonstrated that a higher fluorescence was detected in the brain of mice treated with SLN-mApoE by IT instillation compared to

mice subjected to IP and IV administrations. Intratracheally instilled SLN-mApoE were detectable in the brain and in the lungs up to 24 hours after the administration. Moreover, the analysis of the BAL fluid excluded inflammatory phenomena triggered by SLN-mApoE retention in the lungs.

The administration of NPs by pulmonary route has several advantages: i) the lung has a large surface area; ii) the epithelium of the respiratory zone is thin (barrier thickness decreases from the upper to the lower airways); iii) the pulmonary interstitium is rich of lymphatic and blood vessels. Thank to these properties, NPs can sedimentate or diffuse in the lung according to the aerodynamic diameter. If NPs are able to escape the mucociliary clearance and the macrophage phagocytosis, they retention in the lung is prolonged and they can penetrate the pulmonary epithelium and the interstitium, thus supporting the translocation to other organs, including the brain. [13]

Together, our results promote SLN-mApoE as a good tool to cross the blood-brain barrier and show the possibility to explore the pulmonary route as an alternative strategy for NPs to reach the brain.

Based on these results:

Dal Magro R, Ornaghi F, Cambianica I, Beretta S, Re F, Barbero F, Musicanti C, Donzelli E, Canta A, Masserini M, Cavaletti G, Gasco P, Sancini G. *"Enhanced brain targeting of engineered Solid Lipid Nanoparticles"* (in preparation)

REFERENCES

1. Bana L, Minniti S, Salvati E, Sesana S, Zambelli V, Cagnotto A, et al. Liposomes bi-functionalized with phosphatidic acid and an ApoE-derived peptide affect Aβ aggregation features and cross the blood-brain-barrier: implications for therapy of Alzheimer disease. *Nanomedicine* 2014; 10:1583-90.
2. Balducci C, Mancini S, Minniti S, La Vitola P, Zotti M, Sancini G, et al. Multifunctional liposomes reduce brain β-amyloid burden and ameliorate memory impairment in Alzheimer's disease mouse models. *J Neurosci* 2014; 34:14022-31.
3. Re F, Cambianica I, Zona C, Sesana S, Gregori M, Rigolio R, et al. Functionalization of liposomes with ApoE-derived peptides at different density affects cellular uptake and drug transport across a blood-brain barrier model. *Nanomedicine* 2011; **7**:551-9.
4. Bickel U. How to measure drug transport across the blood-brain barrier. *NeuroRx*. 2005; 2:15-26.
5. Tsurumi C, Esser N, Firat E, Gaedicke S, Follo M, Behe M, Elsässer-Beile U,Grosu AL, Graeser R, Niedermann G. Non-invasive in vivo imaging of tumor-associated CD133/prominin. *PLoS One*. 2010; 5:e15605.
6. Mantecca P, Farina F, Moschini E, Gallinotti D, Gualtieri M, Rohr A, Sancini G, Palestini P, Camatini M. Comparative acute lung inflammation induced by atmospheric PM and size-fractionated tire particles. *Toxicol Lett.* 2010; 198:244-54.
7. Poller B, Gutmann H, Krähenbühl S, Weksler B, Romero I, Couraud PO, Tuffin G, Drewe J, Huwyler J. The human brain endothelial cell line hCMEC/D3 as a human blood-brain barrier model for drug transport studies. *J Neurochem*. 2008; 107:1358-68.
8. Gasco MR. Method for producing solid lipid microspheres having a narrow size distrivution, US Patent 5 250 236 (1993).
9. Müller RH, Rühl D, Runge S, Schulze-Forster K, Mehnert W. Cytotoxicity of solid lipid nanoparticles as a function of the lipid matrix and the surfactant. *Pharm Res*. 1997; 14:458-62.
10. Re F, Cambianica I, Sesana S, Salvati E, Cagnotto A, Salmona M, et al. Functionalization with ApoE-derived peptides enhances the interaction with brain capillary endothelial cells of nanoliposomes binding amyloid-beta peptide. *J Biotechnol* 2010; 156:341-6.

11. Dehouck B, Fenart L, Dehouck MP, Pierce A, Torpier G, Cecchelli R. A new function for the LDL receptor: transcytosis of LDL across the blood-brain barrier. *J Cell Biol*. 1997; 138:877-8
12. Zensi A, Begley D, Pontikis C, Legros C, Mihoreanu L, Wagner S, Büchel C, von Briesen H, Kreuter J. Albumin nanoparticles targeted with Apo E enter the CNS by transcytosis and are delivered to neurones. *J Control Release*. 2009; 137:78-86.
13. Weber S, Zimmer A, Pardeike J. Solid Lipid Nanoparticles (SLN) and Nanostructured Lipid Carriers (NLC) for pulmonary application: a review of the state of the art. *Eur J Pharm Biopharm.* 2014; 86:7-22.

Chapter III

Assessment of the intratracheal instillation as alternative administration route of nanoparticles to reach the brain: potential application for Alzheimer's disease therapy

In this chapter, the lung administration will be exploited as an alternative route for liposomes to reach the brain. We used liposomes functionalized with both mApoE peptide, for brain targeting, and phosphatidic acid, for β-amyloid peptide (Aβ) binding. Aβ peptide is one of the hallmarks of Alzheimer's disease (AD), thus different therapeutic strategies focus to interfere with Aβ deposition. [1] It has already been demonstrated that mApoE-PA-LIP are able i) to cross the BBB *in vitro* and *in vivo*, ii) to bind with high affinity the β-amyloid peptide, iii) to hinder the formation of, and disaggregate, Aβ assemblies, and iv) to reduce brain Aβ burden ameliorating memory impairment in AD mouse models after intraperitoneal administration. [2-4] The interaction among mApoE-PA-LIP, alveolar epithelial cells and macrophages was evaluated by means of *in vitro* experiments. The pharmacokinetics of mApoE-PA-LIP after intratracheal instillation was assessed in healthy mice, whereas their capability to reduce Aβ levels in the brain was evaluated in AD transgenic mice (APP23). APP23 mice overexpress human APP751 carrying the Swedish double mutation, thus resulting in increased total Aβ levels and formation of amyloid plaques. [5]

3.1 METHODS

3.1.1 Preparation and characterization of mApoE-PA-LIP

LIP (mApoE-PA-LIP) composed of Sm and Chol (1:1, M:M) and bi-functionalized with phosphatidic acid (PA) and with the peptide CWG-LRKLRKRLLR (mApoE) derived from the receptor-binding domain (a.a. residues 141-150) of human ApoE, modified by adding the tri-peptide CWG at the C-term, were prepared by Dr Re (University of Milano-Bicocca) as described [2-4] by extrusion procedure using polycarbonate filters (100-nm pore size diameter). mApoE-PA-LIP contained 5 mol % of PA and

1.25 mol % of mApoE. As a control, mono-functionalized LIP with PA (PA-LIP) were also prepared. Radiolabelled ([^{3}H]-Sm and [^{14}C]-PA; 0.001 molar % each) or fluorescent (BODIPY-Sm and Rhod-PE; 0.5 molar % and 1 molar%, respectively) lipids were added as tracers during the preparation. mApoE-PA-LIP were characterized in terms of size, surface charge and stability by means of dynamic light scattering technique. The yield of coupling of mApoE to LIP was assessed by measuring the tryptophan fluorescence intensity (λex = 280nm) of mApoE-PA-LIP before and after purification.

3.1.2 Cell culture and pulmonary epithelium model

Human A549 (pulmonary epithelial cell line) and THP-1 cells (human acute monocytic leukemia cell line) were purchased from ATCC (Milan, Italy). Cells were grown in complete Opti-MEM medium supplemented with GlutaMAX (Gibco, Life Technologies), 10% FBS (Gibco, Life Technologies) and 1% Penicillin-Streptomycin (Life Technologies) and maintained in a humidified atmosphere at 37°C, 5% CO_2. A549 were seeded at a density between $6x10^3$ cells/cm^2 and $1.6x10^4$ cells/cm^2 and grown until confluence. THP-1 cells were seeded at a density of $2\text{-}4x10^5$ cells/ml and diluted every 2-3 days. For uptake studies by confocal microscopy, A549 were grown on 25 mm glass coverslips. For permeability assays, A549 were seeded in 12-well transwell inserts (polyester membrane, 0.4 µm pore size or 3 µm pore size for experiments involving THP-1) at a density of $2.5x10^4$ cells/insert and the culture medium was changed every 2 days. Transwell system allows the formation of two compartments, an apical one (0.5 ml) representative of the alveolar lumen and a basolateral one (1 ml) representative of the blood. Experiments were performed when a constant trans-epithelial electrical resistance (TEER) value was obtained.

3.1.3 Differentiation of THP-1

To induce the differentiation of THP-1 in macrophage-like cells, THP-1 were grown in culture medium supplemented with 8 nM phorbol-12-myristate-13-acetate (PMA, Sigma) for 48 hours at 37°C, 5% CO_2. Differentiated THP-1 cells were detached using 0.05% Trypsin-EDTA solution and seeded in transwell inserts as described below.

3.1.4 Epithelial permeability and uptake of mApoE-PA-LIP

A549, seeded in 12-well transwell inserts, were incubated with increasing amount of dually radiolabelled mApoE-PA-LIP (up to 600 nmol of total lipids/ml) in the upper compartment of the transwell system. For experiments involving THP-1, non-differentiated or differentiated THP-1 were

seeded in the upper chamber of the transwell system at a density of $3x10^5$ cells/ml. Samples were taken from the lower compartment at different time points (up to 3 h) and the radioactivity was measured using a Packard Tricarb 2200CA liquid scintillation analyser (Perkin Elmer). Trans-epithelial permeability (EP) of LIP was calculated as described in chapter 2.1.8. After 3 h, A549 cells were detached from filters using trypsin/EDTA and an aliquot was used to measure the lipid-associated radioactivity content by liquid scintillation counting to determine the mApoE-PA-LIP cellular uptake.

3.1.5 Uptake of mApoE-PA-LIP by THP-1

Monocytic and macrophage-like THP-1 were incubated with [^{14}C]-PA-labelled mApoE-PA-LIP (400 nmol of total lipids/ml) for 3 and 24 hours at 37°C. After the incubation, macrophage-like THP-1 were detached from the support using trypsin/EDTA, while monocytes were harvested. The cell-associated radioactivity was measured by liquid scintillation counting.

3.1.6 Intracellular distribution of mApoE-PA-LIP by confocal microscopy in A549 cells

The intracellular distribution of mApoE-PA-LIP was evaluated by confocal laser scanning microscopy (CLSM). A549 cells were incubated with dually fluorescent mApoE-PA-LIP (100 nmol of total lipids/ml), overnight at 37°C, and fixed with 10% formalin solution. Immunofluorescence technique was used to stain different intracellular compartments, as described in chapter 2.1.6.

3.1.7 Pharmacokinetics and biodistribution of mApoE-PA-LIP

6-8 weeks old BALB/c mice weighting 22-25 g were used for these studies. 100 µl of 40 mM (total lipid concentration) radiolabelled mApoE-PA-LIP, containing 130 µg of PA were administered by IT instillation. Mice (2 mice/experimental group) were sacrificed 3-24-48-72-96 h after instillation. To evaluate mApoE-PA-LIP biodistribution after repeated instillations, 2 mice/experimental group were treated two or three times (48 h part) and sacrificed 24 h after the last instillation. Blood, liver, spleen, kidneys, lungs and brain were collected and solubilized by digestion as described. [6] Radioactivity was measured by a Packard Tricarb 2200CA liquid scintillation counter.

3.1.8 Treatment of transgenic mice

Twelve APPswe single transgenic (APP23) mice 14-16 month-old (Novartis Pharma, Swizerland) were intratracheally (IT) instilled with mApoE-PA-LIP (100 µl, 40mM total lipids, n=6 mice) or with PBS

as a vehicle (100 µl, n=6 mice) once every other day for three weeks. At the end of the treatment, mice were euthanized with an overdose of ketamine/medetomidine (1.75 mg/kg and 1.0 mg/kg respectively) and blood samples were collected by cardiac puncture and treated for plasma separation. Animal brains were dissected, weighed and one hemisphere was fixed and processed for immunohistochemistry; the other hemisphere was processed for Aβ dosage by ELISA assay.

3.1.9 Plaques detection by immunohistochemistry

Brain plaque deposition was examined using the 6E10 monoclonal anti-Aβ antibody (Covance, CA) on 30 µm brain coronal cryostat sections (3 slices/mouse). Brain slices were incubated with blocking solutions for 1 h at RT, then overnight at 4°C with the primary antibodies (6E10 1:500) and finally with the anti-mouse biotinylated secondary antibody (1:200; 1h RT, Vector Laboratories). The immunostaining was developed using the avidin-biotin kit (Vector Laboratories). Tissue analysis and image acquisition were done using an Olympus image analyser and the Cell-R software. Plaques were quantified by an operator blind to genotype and treatment using Fiji software, through the application of a homemade macro.

3.1.10 Brain Aβ quantification by ELISA assay

Mouse brain hemispheres were homogenized in 50 mM TRIS-HCl (pH 7.4), 150 mM NaCl, 50 mM EDTA, 1% Triton X-100 and 2% protease inhibitor, centrifuged at 21000 g, 4°C for 25 min and the supernatant (soluble Aβ) was analysed for Aβ content by ELISA assay (ELISA kit, IBL, Germany). The pellet was then homogenized in 70% formic acid (10% v/w), ultra-centrifuged 100000 g, 4°C, 1 h and the resulting supernatant (insoluble Aβ) was neutralized with 1 M TRIS buffer (pH 11) and analysed for Aβ content by ELISA assay.

3.2 RESULTS

3.2.1 Physicochemical characterization of mApoE-PA-LIP

In this study, we utilized mApoE-PA-LIP previously described. [2-4] DLS analysis showed that LIP were monodispersed (polydispersity index = 0.112), with a size of 141.2 ± 6 nm that remained constant for up to 5 days. The yield of total lipid recovery after extrusion was about 96%. The yield of LIP surface

functionalization with mApoE peptide was 56 ± 7%, according to data already published for this formulation.[7,8]

3.2.2 In vitro model of pulmonary epithelium

TEER values of A549 cells were measured starting from 7 days after seeding in transwell inserts. TEER increased over time starting from 30.7 ± 2.87 $\Omega \times cm^2$. Experiments were performed at day 12 when a maximal TEER value of 54.19 ± 2.58 $\Omega \times cm^2$ was measured.

3.2.3 Epithelial permeability and uptake of mApoE-PA-LIP

The ability of mApoE-PA-LIP to cross the *in vitro* model of pulmonary epithelium was evaluated by radiochemical techniques using dually radiolabelled mApoE-PA-LIP. The EP values of [^{3}H]-Sm ranged from 0.7±0.2 x 10^{-4} to 2.0±0.4 x 10^{-4} cm/min, with a tendency to increase by increasing of the lipid dose. The EP values of [^{14}C]-PA ranged from 3.2±0.9 x 10^{-6} to 9.6±4.8 x 10^{-6} cm/min. The EP of [^{3}H]-Sm was one/two order of magnitude higher compared to the values obtained for [^{14}C]-PA, at each considered lipid dose (Figure 3.1, A). Moreover, after 3 hour of incubation the radioactivity uptaken by the cells increased by increasing the lipid dose of mApoE-PA-LIP reaching saturation at 600 nmols of total lipids/ml (Figure 3.1, B).

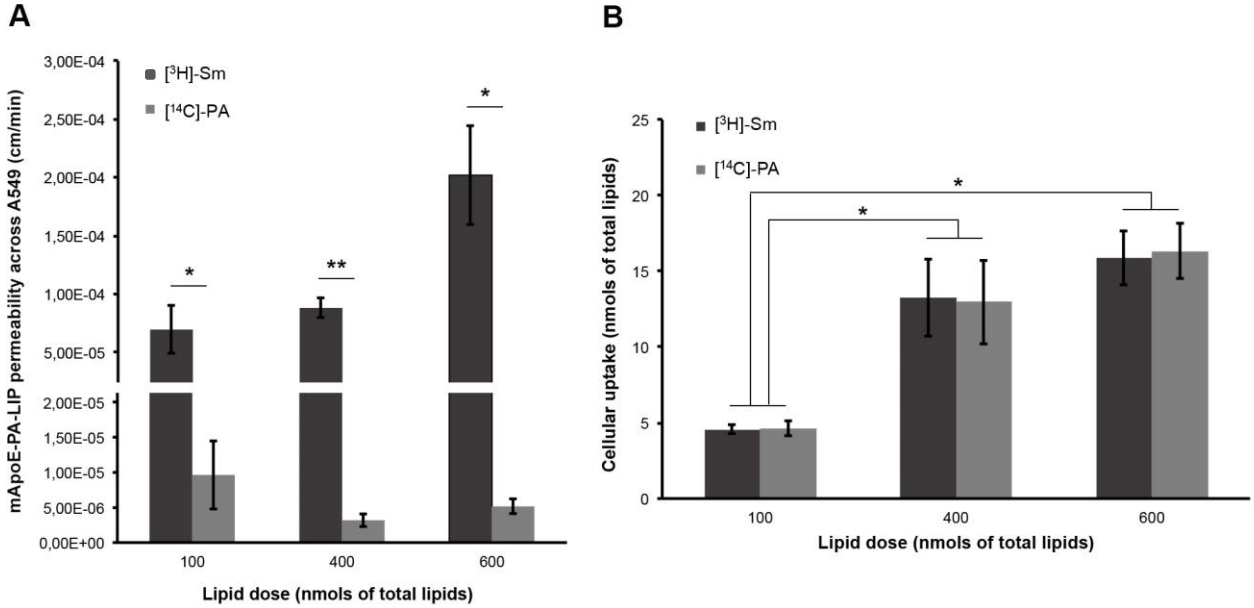

Figure 3.1. Transcellular permeability and uptake of mApoE-PA-LIP by A549 cells. A549 cells were cultured on transwell system and different doses of mApoE-PA-LIP (from 100 to 600 nmols of total lipids/well) were added in the apical compartment. (A) The amount of mApoE-PA-LIP in the basolateral compartment of the transwell system was measured by radiochemical techniques after different incubation times (0-3 h) and the EP values, calculated as described in the methods

section, are shown. (B) 3 h after incubation, cells were collected in a lysis buffer and the lipid-associated radioactivity was measured to determine the mApoE-PA-LIP cellular uptake. The amount of total lipids uptaken from the cells is shown. Experiments have been performed in triplicate. Data are expressed as mean ± SEM; * $p<0.05$; ** $p<0.01$ by Student's *t* test.

The potential role of THP-1 cells as mApoE-PA-LIP transport mediators was evaluated by adding THP-1 cells to the apical compartment of the transwell system together with [^{14}C]-PA-labelled mApoE-PA-LIP. Both monocytes and differentiated THP-1 were used. The EP values of [^{14}C]-PA were higher compared to those reported in Figure 3.1A, with a tendency to increase in presence of macrophage-like THP-1 (Figure 3.2, A).

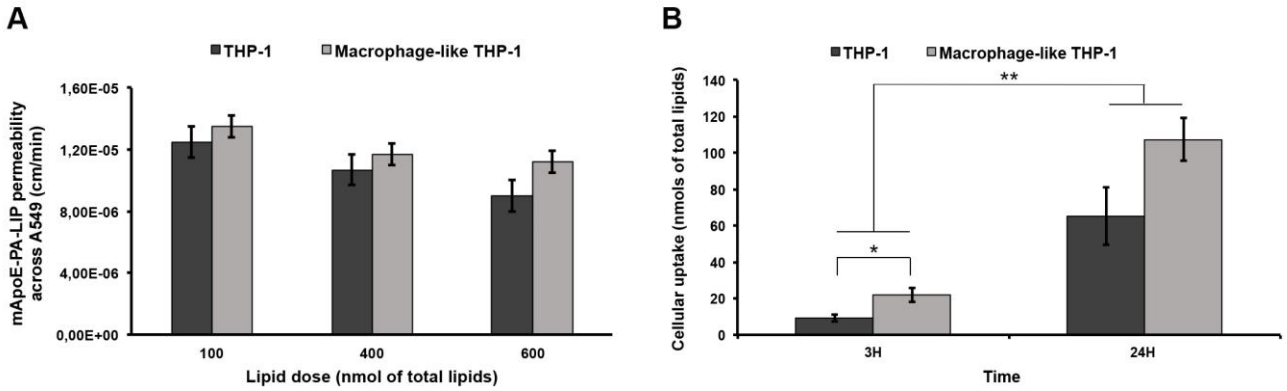

Figure 3.2. Epithelial permeability and uptake of mApoE-PA-LIP in presence of THP-1. (A) Monocytes and macrophage-like THP-1 were added in the apical chamber of the transwell system. Increasing doses of [^{14}C]-PA-labelled mApoE-PA-LIP (from 100 to 600 nmols of total lipids/well) were incubated and the EP values were calculated. (B) THP-1 and differentiated THP-1 were incubated with 400 nmol (total lipids/ml) of radiolabelled mApoE-PA-LIP for 3 and 24 hours. The cell-associated radioactivity was measured to determine the amount of mApoE-PA-LIP uptaken by the cells. Experiments have been performed in triplicate. Data are expressed as mean ± SEM; * $p<0.05$; ** $p<0.01$ by Student's *t* test.

The cellular uptake of mApoE-PA-LIP by THP-1, measured as cell-associated radioactivity, strongly increased over time and after 3 hours of incubation the amount of total lipids associated to macrophage-like THP-1 was about two fold higher respect to the dose uptaken by monocytes (Figure 3.2, B).

3.2.4 Intracellular distribution of mApoE-PA-LIP in A549 cells

The intracellular distribution of dually fluorescent mApoE-PA-LIP (100 nmol of total lipids/ml) in A549 was assessed by CSLM. The co-localization of the two lipid-associated fluorophores suggested that mApoE-PA-LIP entered intact into the cells and that they were mainly located below the plasma membrane of A549 cells (Figure 3.3, A-C).

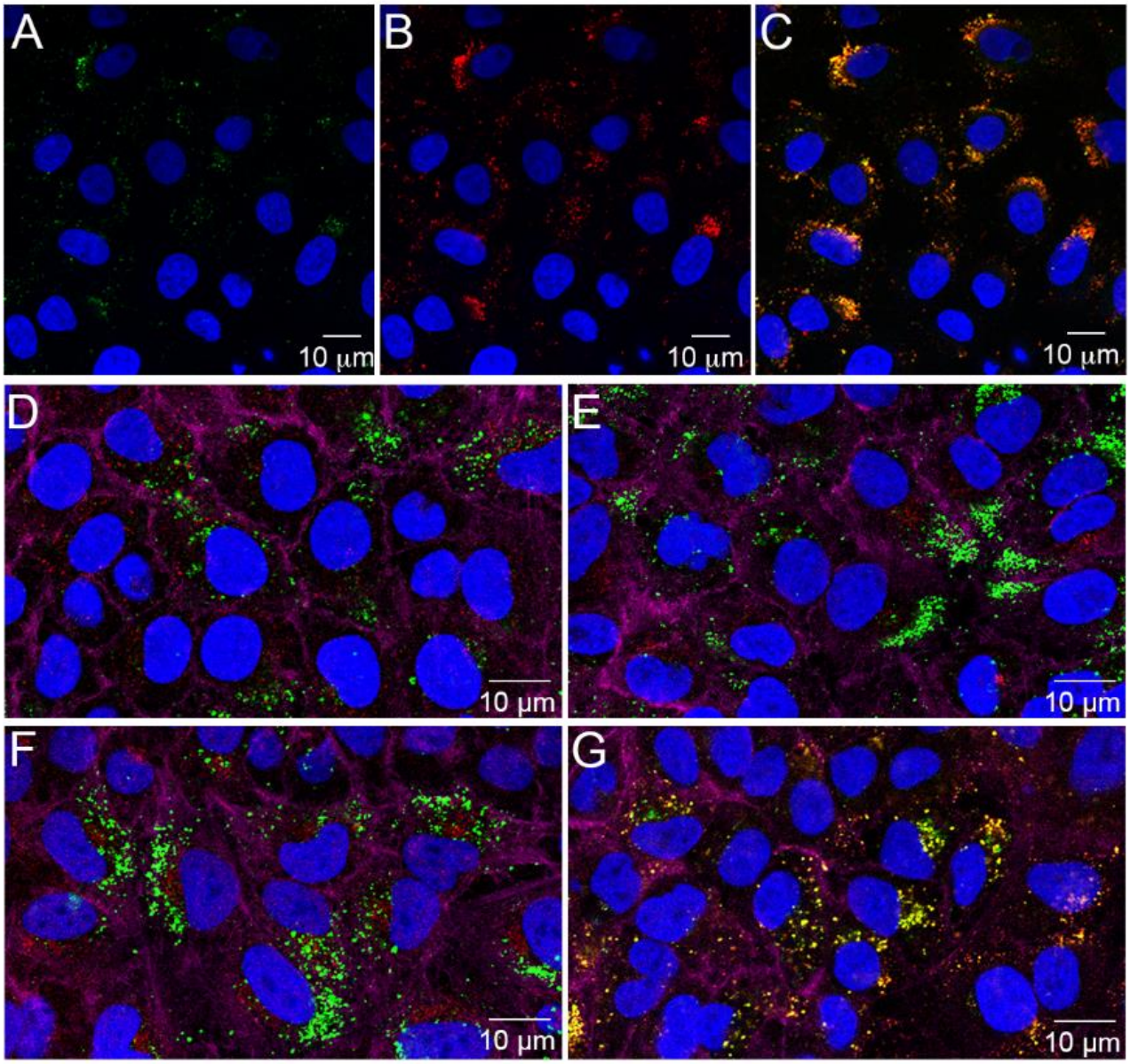

Figure 3.3. Intracellular distribution of mApoE-PA-LIP in A549 cells by confocal microscopy analysis. The intracellular distribution of dually fluorescent mApoE-PA-LIP (100 nmol of total lipids/ml) in A549 was assessed by CSLM after o/n incubation. The intracellular signals of BODIPY-Sm (green fluorescence) and Rhodamine-PE (red fluorescence), used as LIP tracers, are shown (A and B, respectively). The co-localization of the two fluorescent signals (yellow spots) suggested that mApoE-PA-LIP were able to enter intact into the cells (C). The distribution of BODIPY-labelled mApoE-PA-LIP (green fluorescence) in different intracellular organelles (red fluorescence) was also investigated by CLSM. mApoE-PA-LIP did not co-localize with early endosomes (D), late endosomes/lysosomes (E) and recycling vesicles (F). Yellow spots were detected where NP-C1-positive vesicles were stained (G).

Staining of different intracellular organelles and vesicles mainly involved in the degradation pathway or in endocytic recycling of NPs was also performed. The results showed that after over-night incubation with A549 cells, mApoE-PA-LIP did not co-localized neither with early/late endosomes or lysosomes, nor with recycling endosomes (Figure 3.3, D-F). Nevertheless where Niemann-Pick C1 (NPC1) protein was stained, an important co-localization between mApoE-PA-LIP and NPC1 signals was detected (Figure 3.3, G).

3.2.5 Pharmacokinetics and biodistribution of mApoE-PA-LIP

Dually-radiolabelled mApoE-PA-LIP or PA-LIP (as a control) were administered to healthy BALB/c mice by a single IT instillation. At different times after instillation (3-24-48-72-96 h), mice were sacrificed and the radioactivity in the lung, brain, blood, liver, spleen and kidney was measured. High concentration of PA (about 100 µg/g of tissue, corresponding to 30% of the injected dose) was found in the lung (Figure 3.4, A) of mice 24 h after the treatment with PA-LIP or mApoE-PA-LIP. These values remained quite stable up to 48 h and then strongly decreased at $t \geq 72$ h. At the same time points, lower PA amounts in the brain and in the blood were found (Figure 3.4, B-C respectively). PA concentrations in the brain was higher for mApoE-PA-LIP compared to PA-LIP. Notably, the results indicate that the ratio of Sm/PA (11 in original mApoE-PA-LIP sample) was maintained in the lung (10±5 till 72 hours), in the brain (10±6 till 24 hours), but not in the blood samples (30±7). The overall distribution of PA-LIP and mApoE-PA-LIP in the different organs investigated is shown in Table 3.1.

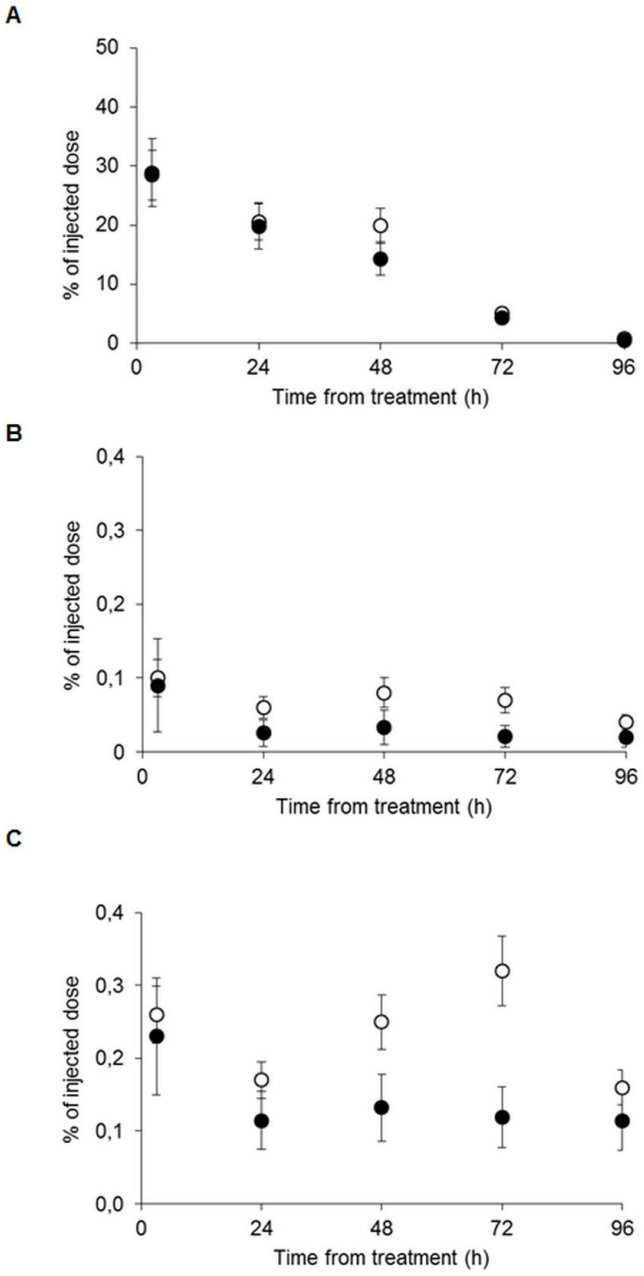

Figure 3.4. Biodistribution of mApoE-PA-LIP and PA-LIP in lung, brain and blood after single IT instillation. Healthy BALB/c mice were IT instilled with dually radiolabelled mApoE-PA-LIP (open circles), or with PA-LIP as a control (filled circles) and at different times after instillation, mice were sacrificed and the radioactivity present in lungs (A), brain (B) and blood (C) was measured by liquid scintillation counting. Data of [^{14}C]-PA radioactivity are expressed as % on injected dose. Data are expressed as mean ± SEM (n=2 mice/group).

Table 3.1 Overall distribution of [^{14}C]-PA radioactivity associated to PA-LIP or mApoE-PA-LIP in the different organs analyzed after single intratracheal instillation (IT) in BALB/c mice.

h after IT injection of PA-LIP

	24h		48h		72h		96h	
	μg PA/organ	% inj. dose	μg PA/organ	% inj. dose	μg PA/organ	% inj. dose	μg PA/organ	% inj. dose
lung	25.20	19.80	18.19	14.30	7.40	4.27	0.60	0.47
brain	0.032	0.030	0.042	0.030	0.022	0.020	0.025	0.020
blood	0.140	0.110	0.160	0.130	0.120	0.120	0.140	0.110
liver	0.380	0.300	0.500	0.400	0.260	0.210	0.310	0.250
spleen	0.020	0.018	0.018	0.014	0.012	0.009	0.010	0.010
kidney	0.120	0.100	0.130	0.110	0.070	0.060	0.090	0.080

h after IT injection of mApoE-PA-LIP

	24h		48h		72h		96h	
	μg PA/organ	% inj. dose	μg PA/organ	% inj. dose	μg PA/organ	% inj. dose	μg PA/organ	% inj. dose
lung	26.12	20.56	25.23	19.86	6.39	5.03	0.57	0.78
brain	0.056	0.060	0.072	0.080	0.066	0.070	0.041	0.040
blood	0.150	0.170	0.220	0.250	0.280	0.320	0.140	0.160
liver	0.880	0.240	0.960	0.310	1.500	1.160	0.610	0.190
spleen	0.020	0.014	0.020	0.011	0.046	0.007	0.020	0.008
kidney	0.160	0.100	0.170	0.010	0.310	0.200	0.150	0.100

In another experiment, mice were subjected to three IT instillations, 48 hours apart, and sacrificed 24 hours after the last instillation of mApoE-PA-LIP or PA-LIP (as a control). The results showed that repeated IT instillations promote an increase in PA concentrations in the brain (Figure 3.5, A) after each instillation. The PA levels measured in the brain were slightly higher than those measured in the blood. Higher PA concentrations in the brain were detected with mApoE-PA-LIP (0.6 μg PA/g brain), compared to the control PA-LIP (0.25 μg PA/g brain).

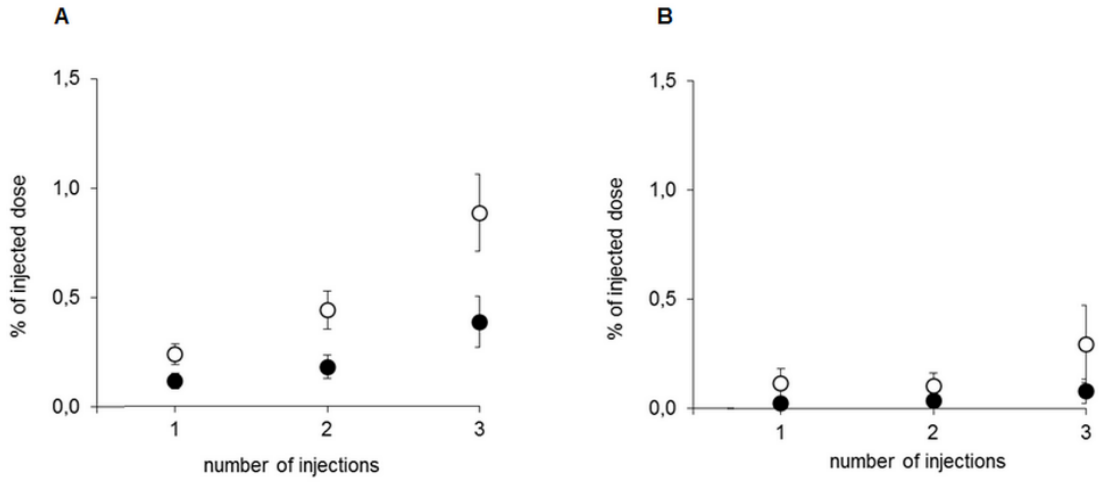

Figure 3.5. *In vivo* brain and blood biodistribution of mApoE-PA-LIP and PA-LIP after repeated IT instillations. Healthy BALB/c mice were IT instilled with dually radiolabelled mApoE-PA-LIP (open circles), or with PA-LIP as a control (filled circles) two or three times (48 h part) and sacrificed 24 h after the last instillation. The radioactivity present in brain (A) and blood (B) was measured by liquid scintillation counting. Data were expressed as % of injected dose. Data of [^{14}C]-PA radioactivity are expressed as mean ± SEM (n=2 mice/group).

3.2.6. In vivo proof-of-principle

In order to assess the *in vivo* proof-of-principle, APP23 mice (n = 6 mice/group) were IT treated with 100 µl, 40 mM total lipids of mApoE-PA-LIP or with 100 µl of PBS (3 instillations/week, once every other day, for 3 weeks). After treatment, mice were sacrificed and blood and brain collected. One brain hemisphere was processed and immunostained for plaque detection. The results showed that whereas APP23 mice treated with PBS (VEH) displayed extracellular plaques (Figure 3.6, A-C) and intracellular Aβ (Figure 3.6, d), in APP23 mice receiving mApoE-PA-LIP by IT instillation plaques were no more detectable (Figure 3.6, E-G) and also intracellular Aβ was completely cleared (Figure 3.6, h-l). No variations in plaque burden were detectable after mouse treatment with PA-LIP (data not shown). Total Aβ levels in brains were quantified by ELISA assay. The results showed that the IT treatment with mApoE-PA-LIP strongly reduced brain $A\beta_{40}$ levels (-72% of reduction) or brain $A\beta_{42}$ levels, although to a lesser extent (-47.3% of reduction), as compared to PBS-treated mice (VEH) (Figure 3.6, M).

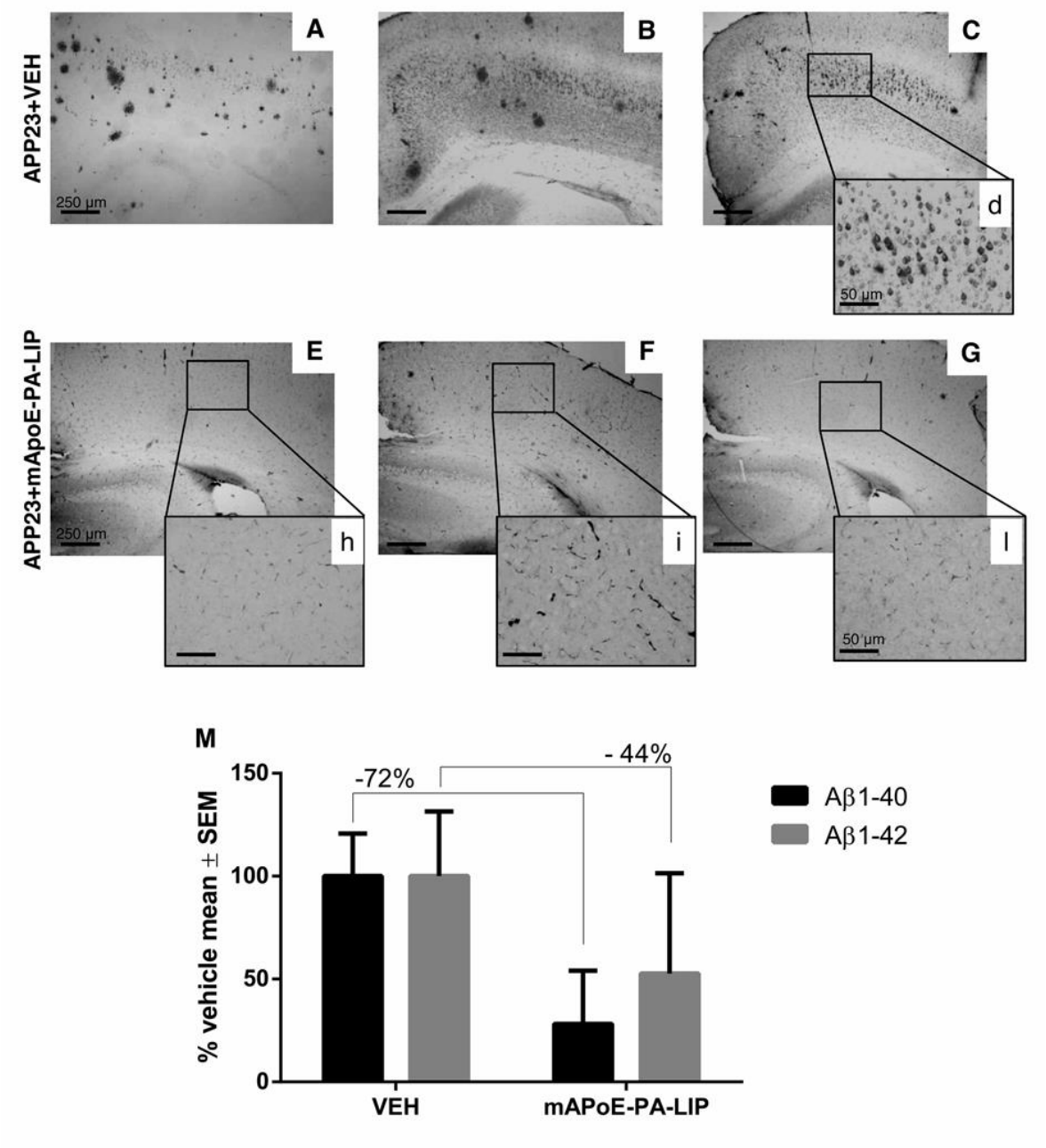

Figure 3.6. IT instillation of mApoE-PA-LIP clears plaques, intracellular Aβ and lowers brain Aβ levels in APP23 mice. Images represents APP23 mouse brain slices immunostained with the anti-Aβ 6E10 monoclonal antibody. As observable, APP23 mice receiving VEH displayed deposited plaques in the brain parenchyma (A-C; scale bar 250 µm) and intracellular Aβ (d; scale bar 50 µm). In contrast, in mice receiving mApoE-PA-LIP treatment plaques were no more detectable (E-G; scale bar 250 µm) and intracellular Aβ has been completely cleared (h-l; scale bar 50 µm). (M) Histograms are % VEH mean ± SEM of insoluble $A\beta_{1-40}$ and $A\beta_{1-42}$ reduction upon mApoE-PA-LIP application in APP23 mice. (n=6 mice/group, vehicle vs mApoE-PA-LIP).

3.3 DISCUSSION

Herein we explore the possibility to use the lung administration as a non-invasive delivery route to enhance the BBB crossing of mApoE-PA-LIP. Indeed these LIP have already been tested both *in vitro,* for their ability to cross a model of BBB, [2] and *in vivo,* demonstrating that mApoE-PA-LIP are able to reach the brain [2] and to reduce Aβ burden in Alzheimer's disease mouse models. [3, 4]

The feasibility of pulmonary route to enhance mApoE-PA-LIP brain targeting was assessed by means of *in vitro* and *in vivo* experiments. A549 cells were used as *in vitro* alveolar epithelium model. Our results show that only a small proportion of mApoE-PA-LIP was able to cross intact the *in vitro* model, although the analysis of the uptake and the intracellular distribution of mApoE-PA-LIP in A549 cells suggested that the majority of mApoE-PA-LIP were unbroken in the cells. A possible explanation comes from the finding that mApoE-PA-LIP displayed an important co-localization with Niemann-Pick C1 (NPC1) protein. NPC1 is a transmembrane protein found in late endosomes and lysosomes and it is responsible of the subcellular trafficking of cholesterol by facilitating the release of lipoprotein-derived sterol from the lumen of lysosomes. Recently, it has been suggested its involvement in the regulation of nanoparticle trafficking and recycling. [9, 10] Moreover, the regulation of cellular cholesterol homeostasis is of particular importance to lung alveolar cells because of the need for production of surfactant with an appropriate lipid composition, [11] and the ability to produce and secrete surfactant has been demonstrated for A549. [12] These findings suggest that the majority of mApoE-PA-LIP uptaken by A549 could be recycled through this pathway, reducing the amount of LIP available for the crossing of the pulmonary epithelium.

Even if nanoparticles translocation across the air-blood barrier seems to exploit mainly transcellular pathways, also paracellular transport might play a role in this process. [13] Therefore we hypothesized a role for macrophages in mApoE-PA-LIP translocation across the pulmonary epithelium. Alveolar macrophages represent the first immune defence encountered by inhaled pathogens in the lower airways and the uptake of NPs by macrophages has been already reported. [14, 15] Our results demonstrate that radiolabelled mApoE-PA-LIP were uptaken by THP-1 in a time dependent manner and that the cell-associated radioactivity increased when differentiated THP-1 were used. Furthermore, the endothelial permeability of mApoE-PA-LIP across A549 was enhanced when THP-1 were added in the apical chamber of the transwell system, suggesting a possible involvement of THP-1 in LIP crossing of the *in vitro* model of pulmonary epithelium.

The *in vivo* pharmacokinetics experiments, carried out in healthy BALB/c mice, showed that after a single IT instillation, mApoE-PA-LIP remained in the lung for more than 48 h, suggesting that they were not removed by mucociliary clearance as hypothesized for other type of NPs. [16] Less than 0.5% of instilled dose reached the blood and less than 0.1% was measured in the brain. The radioactivity detected both in the blood and in the brain remained constant over the time. Nevertheless, the Sm/PA ratio of mApoE-PA-LIP was preserved in the brain (24 h after IT instillation) and in the lung, but strongly increased in the blood after the crossing of the pulmonary epithelium. This observation could suggest that only a small proportion of instilled liposomes are able to cross intact the pulmonary epithelium and that these LIP reach intact the brain.

After repeated IT instillations the amount of PA found in the brain increased after each instillation, whereas the radioactivity detected in the blood was almost unchanged and lower compared to the brain. Higher amount of PA was measured in the brain after treatment with mApoE-PA-LIP compared to PA-LIP. Comparing the results obtained after repeated IT administrations with those previously obtained after repeated IP injections, [3] it is possible to observe that the amount of LIP reaching the brain was similar for both the treatments (~ 0.6% of the injected dose was measured in the brain after the third administration). Indeed, a strong reduction of Aβ (either plaques, intracellular deposition, or total brain Aβ) was achieved at the end of the IT treatment in APP23 mice, as well as in the case of IP administration. [3]

In conclusion, these results support the lung administration of LIP functionalized for brain targeting as an alternative, non-invasive delivery route for NPs to cross the BBB and to reach the brain. Even if the intratracheal administration of particles is less physiological than inhalation exposure, it allows a better control of the administered dose and is a well accepted methodology for the administration of foreign compounds to the airways. [13]

The complete elucidation of LIP translocation from the lung to the brain deserves further investigation as well as the possibility to exploit the pulmonary route by aerosol administration as an alternative strategy for long lasting therapy.

The results have been included in the paper:

Sancini G, Dal Magro R, Ornaghi F, Balducci C, Forloni G, Gobbi M, Salmona M, Re F. *"Lungs as alternative administration route to deliver nanoparticles to the brain: potential application for Alzheimer's disease therapy"* (submitted)

REFERENCES

1. Re F, Gregori M, Masserini M. Nanotechnology for neurodegenerative disorders. *Nanomedicine.* 2012; 8 Suppl 1:S51-8.
2. Bana L, Minniti S, Salvati E, Sesana S, Zambelli V, Cagnotto A, et al. Liposomes bi-functionalized with phosphatidic acid and an ApoE-derived peptide affect Aβ aggregation features and cross the blood-brain-barrier: implications for therapy of Alzheimer disease. *Nanomedicine* 2014; 10:1583-90.
3. Balducci C, Mancini S, Minniti S, La Vitola P, Zotti M, Sancini G, et al. Multifunctional liposomes reduce brain β-amyloid burden and ameliorate memory impairment in Alzheimer's disease mouse models. *J Neurosci* 2014; 34:14022-31.
4. Mancini S, Minniti S, Gregori M, Sancini G, Cagnotto A, Couraud PO, et al. The hunt for brain Aβ oligomers by peripherally circulating multi-functional nanoparticles: Potential therapeutic approach for Alzheimer's disease. *Nanomedicine* 2016; 12:43-52.
5. Sturchler-Pierrat C, Staufenbiel M. Pathogenic mechanisms of Alzheimer's disease analyzed in the APP23 transgenic mouse model. *Ann N Y Acad Sci*. 2000; 920:134-9
6. Wan L, Pooyan S, Hu P, Leibowitz MJ, Stein S, Sinko PJ. Peritoneal macrophage uptake, pharmacokinetics and biodistribution of macrophage-targeted PEG-fMLF (N-formyl-methionyl-leucyl-phenylalanine) nanocarriers for improving HIV drug delivery. *Pharm Res* 2007; 24:2110-9.
7. Re F, Cambianica I, Zona C, Sesana S, Gregori M, Rigolio R, et al. Functionalization of liposomes with ApoE-derived peptides at different density affects cellular uptake and drug transport across a blood-brain barrier model. *Nanomedicine* 2011; 7:551-9.
8. Re F, Cambianica I, Sesana S, Salvati E, Cagnotto A, Salmona M, et al. Functionalization with ApoE-derived peptides enhances the interaction with brain capillary endothelial cells of nanoliposomes binding amyloid-beta peptide. *J Biotechnol* 2010; 156:341-6.
9. Eltoukhy AA, Sahay G, Cunningham JM, Anderson DG. Niemann-Pick C1 affects the gene delivery efficacy of degradable polymeric nanoparticles. *ACS Nano* 2014; 8:7905-13.
10. Sahay G, Querbes W, Alabi C, Eltoukhy A, Sarkar S, Zurenko C, et al. Efficiency of siRNA delivery by lipid nanoparticles is limited by endocytic recycling. *Nat Biotechnol* 2013; 31:653-8.

11. Roszell BR, Tao JQ, Yu KJ, Huang S, Bates SR. Characterization of the Niemann-Pick C pathway in alveolar type II cells and lamellar bodies of the lung. *Am J Physiol Lung Cell Mol Physiol*. 2012; 302:L919-32.
12. Klein SG, Serchi T, Hoffmann L, Blömeke B, Gutleb AC. An improved 3D tetraculture system mimicking the cellular organisation at the alveolar barrier to study the potential toxic effects of particles on the lung. *Part Fibre Toxicol*. 2013; 10:31.
13. Kreyling WG, Hirn S, Möller W, Schleh C, Wenk A, Celik G, Lipka J, Schäffler M, Haberl N, Johnston BD, Sperling R, Schmid G, Simon U, Parak WJ, Semmler-Behnke M. Air-blood barrier translocation of tracheally instilled gold nanoparticles inversely depends on particle size. *ACS Nano.* 2014; 8:222-33.
14. Liu YX, Karsai A, Anderson DS, Silva RM, Uyeminami DL, Van Winkle LS, Pinkerton KE, Liu GY. Single-Cell Mechanics Provides an Effective Means To Probe in Vivo Interactions between Alveolar Macrophages and Silver Nanoparticles. *J Phys Chem B*. 2015; 119:15118-29.
15. Markus MA, Napp J, Behnke T, Mitkovski M, Monecke S, Dullin C, Kilfeather S, Dressel R, Resch-Genger U, Alves F. Tracking of Inhaled Near-Infrared Fluorescent Nanoparticles in Lungs of SKH-1 Mice with Allergic Airway Inflammation. *ACS Nano*. 2015; 9:11642-57.
16. Geiser M, Kreyling WG. Deposition and biokinetics of inhaled nanoparticles. *Part Fibre Toxicol* 2010; **7**:2.

Chapter IV

Artificial apolipoprotein-E4 corona enables nanoparticles brain targeting

In this chapter an intriguing alternative to covalent functionalization of nanoparticles (NPs) surface with brain targeted ligands will be proposed. Indeed, the covalent functionalization of NPs with biomolecules that bind receptors expressed on BBB luminal side is the most exploited strategy to enhance NPs brain targeting. There is now a large amount of evidences that this strategy can increase several times the amount of drugs delivered to the brain parenchyma but no products have reached the clinic yet. [1] Among the different issues that hindered the clinical development of nanotechnology-based carriers for brain targeting, one is surely the complexity to shift the set of chemical reactions required for the covalent functionalization of NPs from the laboratory scale to a large scale. [1]

We used polysorbate 80-coated solid lipid nanoparticles, here referred as Lipid NPs, which have already been characterized in terms of long-term stability, lack of *in vivo* toxicity and ability to cross the blood-brain barrier (BBB). The Lipid NPs tropism for the BBB has been previously demonstrated for other polysorbate 80-coated formulations and it depends on the adsorption of certain apolipoproteins on the NPs surface, induced by the presence of this specific surfactant. [2, 3]

Here Lipid NPs have been decorated with an artificial protein corona made of apoliprotein E, prepared extemporaneously, and their capability to reach the brain has been assessed after intravenous administration to healthy mice.

4.1 METHODS

4.1.1 Lipid nanoparticles preparation

Lipid NPs were prepared by Dr Paolo Blasi (University of Camerino, Italy) using the hot high pressure homogenization technique already reported with some modification. [4] Cetilpalmitate (0.8 g) was melted at 65°C and slowly added to 40 mL of polysorbate 80 (0.2% w/v) saline solution (conditioned at 65°C)

under high-speed stirring (8000 rpm) (Ultra Turrax T25 IKA® Werke GmbH & Co. KG). This pre-emulsion was then processed with a high pressure homogenizer (Avestin Emulsiflex C5) at the same temperature for 7 times at 1500 bar. To prepare nile red-loaded or DiR-loaded lipid NPs, nile red (0.5 mg) or DiR (50 µM) were dispersed in the molten lipid in the dark and allowed to dissolve under stirring. Lipid NPs have been sterilized using a polyvinylidene fluoride (PVDF) membrane (porosity 0.45 µm, Millipore Corporation). The hot emulsion was sampled with a 20 mL glass syringe (Perfectum®, Popper & Sons Inc) and filtered. The vial was finally cooled in an ice bath under mild agitation.

4.1.2 Particle size and morphology determination

Photon correlation spectroscopy (PCS) analysis was performed in triplicate at 20°C for 15 min to determine particle size. A Nicomp 380 autocorrelator (PSS Inc.) equipped with a Coherent Innova 70-3 (Laser Innovation) argon ion laser was used for PCS measurements. Samples were prepared adding 2 µL of the Lipid NPs suspension to 3 mL of ultrapure water. Lipid NPs were morphologically characterized using transmission electron microscopy (TEM) and scanning electron microscopy (SEM). Samples were prepared by allowing a drop of the lipid NPs suspension to dry overnight on the surface of a 200 mesh Formvar® coated copper grid (TAAB Laboratories Equipment Ltd.)

4.1.3 Artificial ApoE corona

Lipid NPs were incubated for 15 minutes at 37 °C with increasing concentrations of apolipoprotein-E3 (ApoE3) and apolipoprotein-E4 (ApoE4), corresponding to 5, 10 e 20 µg of protein per mL of Lipid NPs suspension. Immediately after the incubation, the obtained Lipid NPs-ApoE3 or -ApoE4 were utilized for *in vivo* experiments.

4.1.4 In vivo treatments

BALB/c mice, 6-8 weeks old, were randomly divided in seven groups (2 mice per group) and intravenously (IV) administered with 100 µl of Lipid NPs loaded with 50 µM DiR. The group 1 was treated with non-functionalized Lipid NPs, groups 2, 3 and 4 were subjected to IV administration of Lipid NPs-ApoE3 (ApoE3: 5, 10 or 20 µg/ml), whereas Lipid NPs-ApoE4 (ApoE4: 5, 10 or 20 µg/ml) were administered to the last three groups (5, 6 and 7). The lipid-associated fluorescence in the brain was evaluated 30 minutes after the injection by means of Fluorescence Molecular Tomography system (FMT1500), as described in chapter 2.1.9. The biodistribution of the most promising formulation was

assessed increasing the number of mice (6 mice per group, Lipid NPs vs Lipid NPs-ApoE4-treated mice).

4.1.5 Brain slices preparation and immunohistochemistry

Seven BALB/c mice were treated with 100 µl of nile red-loaded Lipid NPs-ApoE4 (5 µg of ApoE4/ml of Lipid NPs) by IV administration. Thirty minutes after the administration, mice were euthanized by cervical dislocation and brains were collected and fixed in 10% formalin solution. Brains were cut into coronal 100 µm sections using a microtome (Electron Microscopy Sciences). For immunohistochemistry assay, floating sections were incubated with primary rabbit polyclonal GFAP antibody (Dako, Milano, Italy) diluted 1:500 in 1% NGS, 0,1% BSA, 0,1% Triton X-100 in PBS for 24 hours at 4°C, under gentle agitation. Brain slices were rinsed with PBS buffer, incubated with Alexa Fluor 488 goat anti-rabbit (1:600 in NGS 1%, BSA 0,1% in PBS) for 2 hours at room temperature under continuous agitation, washed in PBS and mounted on microscope slides using ProLong Gold antifade reagent.

4.2 RESULTS

4.2.1 Lipid NPs physical characterization

Lipid NPs already described and characterized for long-term stability [5] have been utilized. Lipid NPs had a mean hydrodynamic diameter (M.H.D) of about 180 nm and a weakly positive z-potential. The absorption of ApoE3 or ApoE4 on the surface of Lipid NPs was related to an increase of the Lipid NPs M.H.D and slightly negative z-potential values (Figure 4.1, A). The results obtained by TEM and SEM analysis are shown in Figure 4.1, B-C.

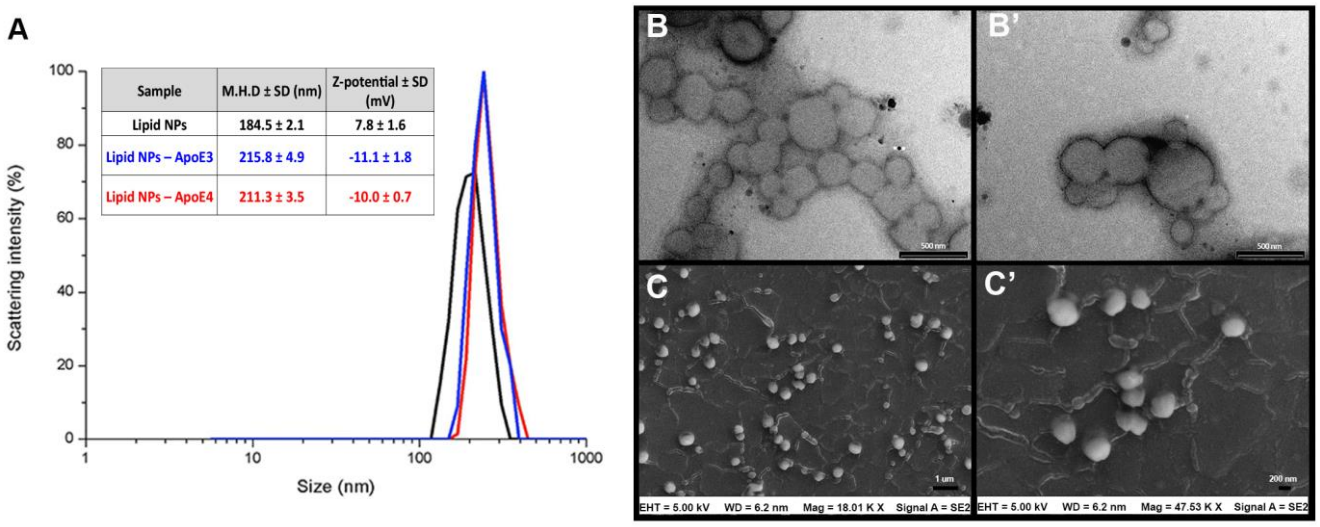

Figure 4.1. Lipid NPs characterization. A) Lipid NPs, Lipid NPs-ApoE3 (20 µg/ml) and Lipid NPs-ApoE4 (5 µg/ml) size and z-potential measured by PCS. B) Lipid NPs spherical shape visualized by TEM (B, magnification B') and SEM (C, magnification C') analysis.

4.2.2 Lipid-associated fluorescence in the brain

The capability of an artificial single protein (ApoE3 or ApoE4) corona to increase Lipid NPs brain targeting was assessed by means of FMT1500. DiR-loaded non-functionalized Lipid NPs and Lipid NPs incubated with increasing amounts of ApoE3 or ApoE4 were administered to mice by IV injection and after 30 minutes the lipid-associated fluorescence in the brain was detected and quantified. Among the different tested formulation, Lipid NPs–ApoE4 (ApoE4 concentration: 5 µg/ml) provided a 3-fold increase of fluorescence in the brain, compared to Lipid NPs and Lipid NPs-ApoE3 (Table 4.1). A dose dependent increase of lipid-associated fluorescence was observed by increasing the amount of ApoE3 incubated with Lipid NPs, but the percentage of DiR-loaded Lipid NPs-ApoE3 (20 µg/ml) in the brain was comparable to the fluorescence displayed by Lipid NPs. On the contrary, in the case of Lipid NPs-ApoE4, the fluorescence in the brain decreased when Lipid NPs were incubated with larger amount of ApoE4.

Table 4.1. DiR fluorescence (% of the injected dose) in the brain 30 minutes after IV administration.

	Fluorescence in the brain (%)
Free fluorophore	0
Lipid NPs	1.08
Lipid NPs-ApoE3 (5 µg/ml)	0.79
Lipid NPs-ApoE3 (10 µg/ml)	1.40
Lipid NPs-ApoE3 (20 µg/ml)	1.75
Lipid NPs-ApoE4 (5 µg/ml)	3.43
Lipid NPs-ApoE4 (10 µg/ml)	0.82
Lipid NPs-ApoE4 (20 µg/ml)	0.13

As shown in Figure 4.2, thirty minutes after the IV injection the fluorescence displayed by Lipid NPs-ApoE4 (ApoE4 = 5 µg/ml) was significantly higher compared to Lipid NPs.

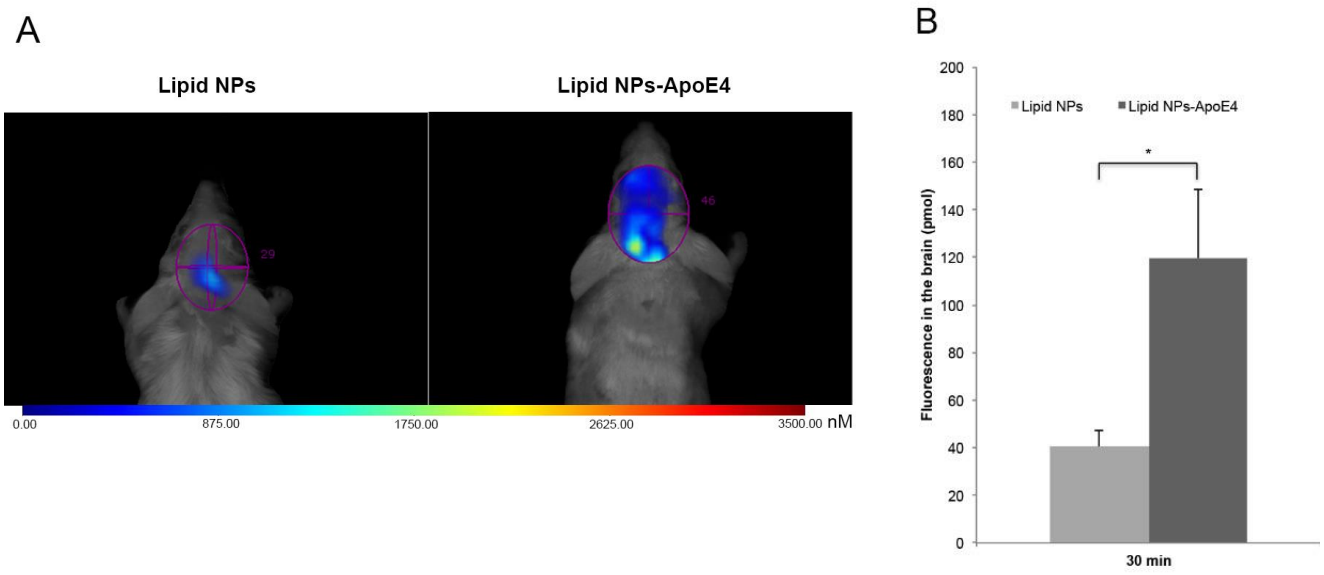

Figure 4.2. Comparison between Lipid NPs and Lipid NPs-ApoE4-associated fluorescence in the brain. (A) Mice were intravenously administered with 100 µl of DiR-loaded Lipid NPs or Lipid NPs-ApoE4 (ApoE4 = 5 µg/ml) and each mouse was analysed 30 minutes after the administration. (B) Amount of DiR (pmol) in the selected ROI. Thirty minutes after IV injection, mice treated with Lipid NPs-ApoE4 (heavy grey bars) showed a significant increment of the brain fluorescence compared to those administered with Lipid NPs (light grey bars). Data are expressed as mean ± SEM; * $p<0.01$ by Student's *t* test (n=6 mice/group, Lipid NPs vs Lipid NPs-ApoE4).

4.2.3 Lipid NPs-ApoE4 distribution in the brain

The capability of nile red-loaded Lipid NPs-ApoE4 (5 µg/ml) to reach the brain parenchyma was evaluated by CLSM. The staining of glial fibrillary acidic protein was performed in order to identify the coverage of blood vessels by astrocytic perivascular processes. Thirty minutes after the IV administration, Lipid NPs-ApoE4 were clearly located both in the brain parenchyma and within the brain blood vessels (Figure 4.3).

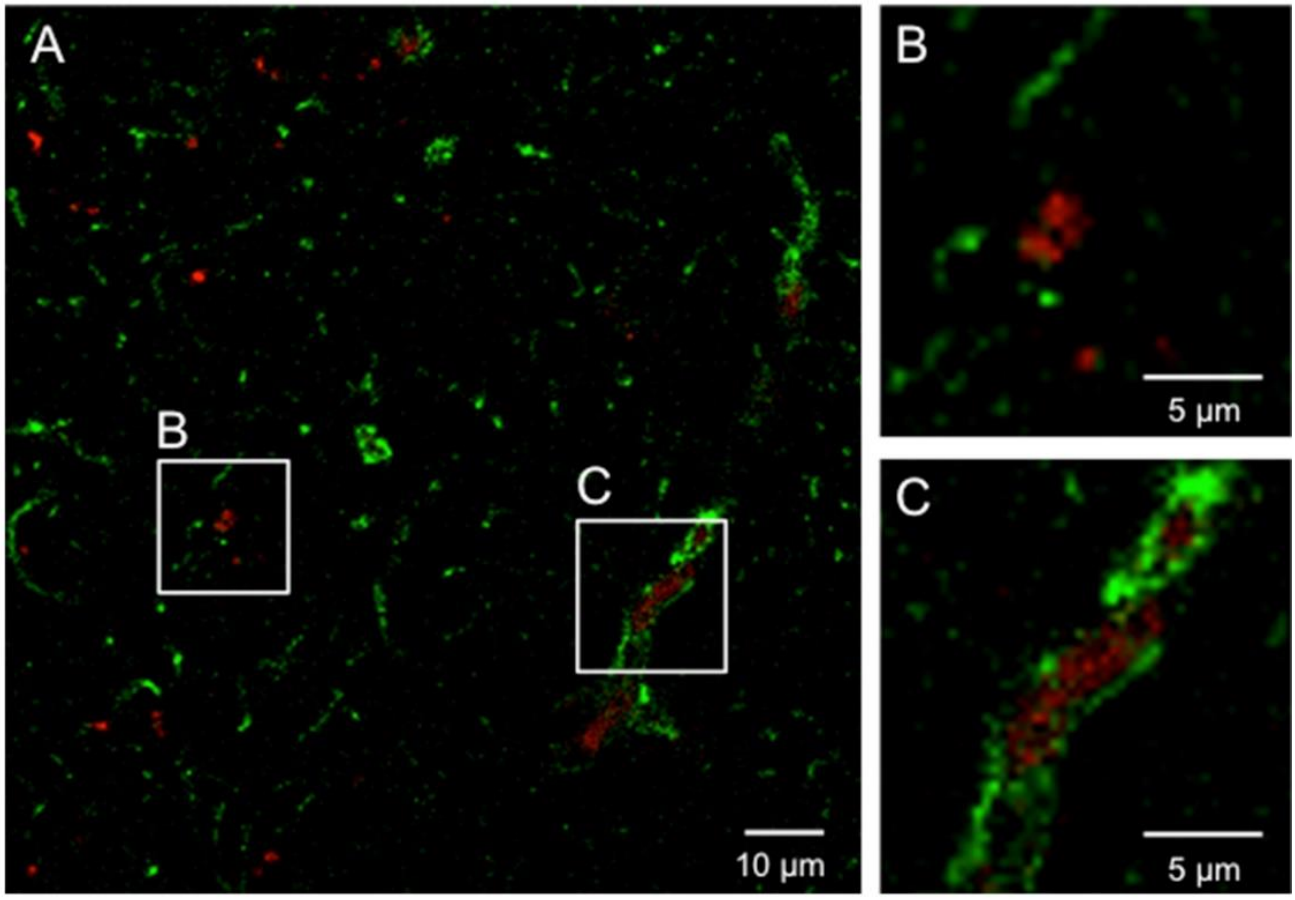

Figure 4.3. Lipid NPs-ApoE4 distribution in cortex. (A) 30 minutes after the IV administration of nile red-loaded Lipid NPs-ApoE4 (red spots), the fluorescence was detectable both in brain capillaries and in the brain parenchyma. Astrocyte intermediate filaments were stained using anti-GFAP antibody (green signal). (B) Magnification of Lipid NPs-ApoE4 aggregates in brain parenchyma. (C) Magnification of Lipid NPs-ApoE4 in cerebral blood capillaries.

4.3. DISCUSSION

In this study we explore the possibility to functionalize the surface of polysorbate 80-coated solid lipid nanoparticles, here referred as Lipid NPs, with an artificial protein corona made of apolipoprotein E in order to enhance their brain targeting.

Polysorbate 80-coated NPs have been utilized to transport different drugs, such as the peptide dalargin, [2] loperamide, [6, 7] doxorubicin [8, 9] as well as other drugs across the BBB. It has been demonstrated that after administration in the systemic circulation, the brain accumulation of polysorbate 80-coated NPs was fast and significantly higher compared to the same formulation without polysorbate-80 coating. The putative mechanism was credited to a preferential adsorption of certain circulating apolipoproteins, mainly ApoE, ApoB-100 and ApoA-I on the surface of NPs. [3, 10, 11] Exploiting this protein corona effect, polysorbate 80-coated NPs may mimic circulating lipoproteins, thus avoiding sequestration by the mononuclear phagocyte system (MPS) and taking advantage of receptor-mediated endocytosis pathways to cross the BBB. This specific feature may be mainly linked to ApoE interaction with LDL receptors, including LDL-R [7, 12] and LRP, [13, 14] that are present on capillary endothelial cells of several species and whose expression is up-regulated at the BBB respect to peripheral vessels. [7, 15]

Here we used polysorbate 80-coated Lipid NPs prepared by hot high pressure homogenization technique as previously described. [5] Blasi and colleagues reported that this formulation has a long-term stability when Lipid NPs are stored at 4°C (> 4 years). The *in vivo* biocompatibility of Lipid NPs has been evaluated both in chicken embryos and in rats without evidences of toxicity. Moreover, thirty minutes after intravenous administration polysorbate 80-coated Lipid NPs have been observed within cerebral capillaries and brain parenchyma. [5] Thanks to these previous findings, *in vitro* evaluations of Lipid NPs toxicity and ability to cross blood-brain barrier models were sidestepped and fluorescence molecular tomography (FMT) was exploited to perform a high-throughput screening among different surface-modified Lipid-NPs.

We performed a non-covalent functionalization of Lipid NPs with two isoforms of ApoE, ApoE3 and ApoE4, which have 100% receptor binding affinity. [16] The third human apolipoprotein E isoform, ApoE2, was discarded due to its low affinity for LDL receptor (<1%). [16]

Increasing amount of ApoE3 and ApoE4 were incubated with the Lipid NPs dispersion for 15 minutes at 37°C and immediately administered to healthy mice by intravenous injection. Thirty minutes after the injection, the lipid-associated fluorescence appeared in the brain. This result is in accordance with previous findings concerning polysorbate 80-coated NPs capability to reach the brain 15-30 minutes

after the administration. [5, 17, 18] The highest fluorescence was detected when Lipid NPs were incubated with the lowest concentration of ApoE4 (5 µg/ml), whereas a reduction of Lipid NPs accumulation in the brain was observed when the particles were incubated with increasing amount of ApoE4. This finding could suggest a saturation of ApoE4 adsorption sites on the surface of polysorbate 80-coated Lipid NPs, resulting in the binding of the free amount of ApoE4 to LDL receptors, thus reducing Lipid NPs-ApoE4 transcytosis. This issue deserves further investigations.

Thirty minutes after Lipid NPs-ApoE4 (ApoE4 = 5 µg/ml) administration, mice were euthanized and brains were collected to examine Lipid NPs distribution in the cerebral cortex. Lipid-associated fluorescence was detected both in cerebral capillaries and in the brain parenchyma, thus confirming Lipid NPs capability to cross the BBB.

In conclusion we demonstrated that an artificial apolipoprotein E4 corona, prepared extemporaneously, increases Lipid NPs brain targeting. Therefore, the use of an artificial protein corona could be an elegant alternative to decorate the surface of NPs with targeted proteins or peptide, shortening the time needed from bench to bed. Indeed, functionalization done through covalent bonds is complex to perform on large scale production because it requires multiple synthesis and quality control steps, thus increasing the time and the cost of production.

Based on these results:

Dal Magro R, Albertini B, Beretta S, Donzelli E, Chiorazzi A, Cavaletti G, Blasi P, Sancini G. "*Artificial Apolipoprotein-E4 Corona Enables Nanoparticles Brain Targeting*". (in preparation)

REFERENCES

1. Sercombe L, Veerati T, Moheimani F, Wu SY, Sood AK, Hua S. Advances and Challenges of Liposome Assisted Drug Delivery. *Front Pharmacol*. 2015; 6:286.
2. Kreuter J, Alyautdin RN, Kharkevich DA, Ivanov AA. Passage of peptides through the blood-brain barrier with colloidal polymer particles (nanoparticles). *Brain Res*. 1995; 674:171-4.
3. Göppert TM, Müller RH. Polysorbate-stabilized solid lipid nanoparticles as colloidal carriers for intravenous targeting of drugs to the brain: comparison of plasma protein adsorption patterns. *J Drug Target.* 2005; 13:179-87.
4. Blasi P, Giovagnoli S, Schoubben A, Puglia C, Bonina F, Rossi C, Ricci M. Lipid nanoparticles for brain targeting I. Formulation optimization. *Int J Pharm*. 2011; 419:287-95.
5. Blasi P, Schoubben A, Traina G, Manfroni G, Barberini L, Alberti PF, Cirotto C, Ricci M. Lipid nanoparticles for brain targeting III. Long-term stability and in vivo toxicity. *Int J Pharm*. 2013; 454:316-23.
6. Alyautdin RN, Petrov VE, Langer K, Berthold A, Kharkevich DA, Kreuter J. Delivery of loperamide across the blood-brain barrier with polysorbate 80-coated polybutylcyanoacrylate nanoparticles. *Pharm Res*. 1997; 14:325-8.
7. Michaelis K, Hoffmann MM, Dreis S, Herbert E, Alyautdin RN, Michaelis M, Kreuter J, Langer K. Covalent linkage of apolipoprotein e to albumin nanoparticles strongly enhances drug transport into the brain. *J Pharmacol Exp Ther*. 2006; 317:1246-53.
8. Gulyaev AE, Gelperina SE, Skidan IN, Antropov AS, Kivman GY, Kreuter J. Significant transport of doxorubicin into the brain with polysorbate 80-coated nanoparticles. *Pharm Res*. 1999; 16:1564-9.
9. Ambruosi A, Yamamoto H, Kreuter J. Body distribution of polysorbate-80 and doxorubicin-loaded [^{14}C]-poly(butyl cyanoacrylate) nanoparticles after i.v. administration in rats. *J Drug Target*. 2005; 13:535-42.
10. Sempf K, Arrey T, Gelperina S, Schorge T, Meyer B, Karas M, Kreuter J. Adsorption of plasma proteins on uncoated PLGA nanoparticles. *Eur J Pharm Biopharm*. 2013; 85:53-60.
11. Petri B, Bootz A, Khalansky A, Hekmatara T, Müller R, Uhl R, Kreuter J, Gelperina S. Chemotherapy of brain tumour using doxorubicin bound to surfactant-coated poly(butyl cyanoacrylate) nanoparticles: revisiting the role of surfactants. *J Control Release*. 2007; 117:51-8.

12. Kreuter J. Influence of the surface properties on nanoparticle-mediated transport of drugs to the brain. *J Nanosci Nanotechnol*. 2004; 4:484-8.
13. Croy JE, Brandon T, Komives EA. Two apolipoprotein E mimetic peptides, ApoE (130-149) and ApoE $(141\text{-}155)_2$, bind to LRP1. *Biochemistry*. 2004; 43:7328-35.
14. Nayyar G, Handattu SP, Monroe CE, Chaddha M, Datta G, Mishra VK, Keenum TD, Palgunachari MN, Garber DW, Anantharamaiah GM. Two adjacent domains (141-150 and 151-160) of apoE covalently linked to a class A amphipathic helical peptide exhibit opposite atherogenic effects. *Atherosclerosis.* 2010; 213:449-57.
15. Dehouck B, Fenart L, Dehouck MP, Pierce A, Torpier G, Cecchelli R. A new function for the LDL receptor: transcytosis of LDL across the blood-brain barrier. *J Cell Biol*. 1997; 138:877-89.
16. Huang Y, Mahley RW. Apolipoprotein E: structure and function in lipid metabolism, neurobiology, and Alzheimer's diseases. *Neurobiol Dis*. 2014; 72 Pt A:3-12.
17. Kreuter J, Hekmatara T, Dreis S, Vogel T, Gelperina S, Langer K. Covalent attachment of apolipoprotein A-I and apolipoprotein B-100 to albumin nanoparticles enables drug transport into the brain. *J Control Release*. 2007; 118:54-8.
18. Zensi A, Begley D, Pontikis C, Legros C, Mihoreanu L, Wagner S, Büchel C, von Briesen H, Kreuter J. Albumin nanoparticles targeted with Apo E enter the CNS by transcytosis and are delivered to neurones. *J Control Release*. 2009; 137:78-86

Conclusions

Nanoparticles-based strategies represent a non-invasive promising approach to overcome the blood-brain barrier. Among the different nanoparticles (NPs) formulations, lipid-based nanoparticles have some advantageous properties such as biocompatibility, biodegradability, low toxicity and the possibility to modify their surface with ligands in order to obtain a site specific targeting of the payload.

Here we exploited apolipoprotein E binding affinity to low-density lipoprotein receptors, highly expressed on brain capillary endothelial cells, to increase nanoparticles brain targeting and BBB crossing. Our results suggest that the covalent functionalization of both solid lipid nanoparticles (SLN) and liposomes (LIP) with mApoE enhances their access to the brain. Moreover, we assessed the suitability of lung administration as an alternative administration route for brain targeted nanoparticles. We demonstrated that both SLN-mApoE and mApoE-PA-LIP accumulate in the brain after intratracheal instillation, thus suggesting the existence of translocation pathways from the lungs to the brain that might be exploited for implementing further strategies for drug delivery to the brain.

We also assessed an innovative approach to decorate the surface of nanoparticles avoiding the covalent conjugation of ligands. Exploiting the high affinity between polysorbate 80 and ApoE, brain targeted solid lipid nanoparticles were prepared and intravenously administered to mice. Our results demonstrate that Lipid NPs-ApoE4 quickly reach the brain parenchyma, thus suggesting the suitability of this strategy for future applications.

In conclusion, all the tested lipid-based formulation have shown enhanced brain targeting after surface functionalization with ApoE (or ApoE-derived peptide), confirming the efficacy of this tailoring to produce drug delivery systems able to cross the BBB.

Acknowledgments

At the end of this work I would like to thank all the people I have met during these wonderfull three years; each of you has enriched my experience as a young scientist.

My deepest gratitude goes to my supervisor, Dr Giulio Sancini, who has always believed in me since I started my master thesis in his laboratory. Thanks for being my mentor and taking care of me in this "jungle".
I am also extremely grateful to all the scientists that contributed to this thesis with their work. I would like to thank Dr Paolo Gasco, Dr Claudia Musicanti, Dr Barbara Albertini and Dr Paolo Blasi for the synthesis and characterization of the solid lipid nanoparticles and for introducing me to the quite obscure world of the nanoparticles manufacturing.
Thanks to Dr Francesca Re for providing liposomes and, togheter with Dr Marco Gobbi and Dr Claudia Balducci, for *in vivo* experiments using LIP.
I thank Dr Roberta Rigolio for FACS analysis and I am grateful to Dr Elisabetta Donzelli, Dr Annalisa Canta and Dr Alessia Chiorazzi for *in vivo* treatments and FMT1500 analysis.

Special thanks to people who shared with me this experience, it would not have been so exciting without you. Thanks to Francesca, who took care of me during my first year of PhD and has been an excellent teacher and fellow. Thanks to my chick Silvia and to Giada for their affection, even though we spent only one year together you are special friends. My sincere thanks to Anna and Gaia, we have walked side by side during these years, through successes and failures, and we spent the most beautiful moments together. Thanks for supporting me at work and especially in my private life.

All of my gratitude goes to my lovely family, who made me the person who I am. Thanks to mom and dad for having always believed in me and supported all my choices. Thanks to my grandmother, who lighted a candle to help me pass each exams of my career. Your memory will warm up forever my heart. The most special thanks is for my husband, my biggest supporter, who has wonderfully changed my life.